galaxies

MDPI

Article

Asteroseismic Analysis of δ Scuti Components of Binary Systems: The Case of KIC 8504570

Alexios Liakos [1,*] and Panagiotis Niarchos [2]

[1] Institute for Astronomy, Astrophysics, Space Applications and Remote Sensing, National Observatory of Athens, Metaxa & Vas. Pavlou St., Penteli, 15236 Athens, Greece
[2] Section of Astrophysics, Astronomy and Mechanics, Department of Physics, National and Kapodistrian University of Athens, Zografos, 15784 Athens, Greece; pniarcho@phys.uoa.gr
* Correspondence: alliakos@noa.gr

Received: 22 September 2020; Accepted: 20 October 2020; Published: 28 October 2020

Abstract: The present work concerns the Asteroseismology of the *Kepler*-detached eclipsing binary KIC 8504570. Particularly, it focuses on the pulsational behaviour of the oscillating component of this system and the estimation of its physical parameters in order to enrich the so far poor sample of systems of this kind. Using spectroscopic observations, the spectral type of the primary component was determined and used to create accurate light curve models and estimate its absolute parameters. The light curve residuals were subsequently analysed using Fourier transformation techniques to obtain the pulsation models. Theoretical models of δ Scuti stars were employed to identify the oscillation modes of the six detected independent frequencies of the pulsator. In addition, more than 385 combination frequencies were also detected. The absolute and the pulsational properties of the δ Scuti star of this system are discussed and compared with all the currently known similar cases. Moreover, using a recent(empirical) luminosity–pulsation period relationship for δ Scuti stars, the distance of the system was estimated.

Keywords: stars binaries; eclipsing; fundamental parameters; binaries; close oscillations; delta Scuti; oscillations; individual; KIC 8504570

1. Introduction

The δ Scuti stars are short-period and multiperiodic pulsating variables. In general, they oscillate in radial and low-order non-radial pulsations due to κ-mechanism [1,2]. However, recently, it has been proposed that the turbulent pressure in the hydrogen convective zone may explain the observed high-order non-radial modes [3,4]. Their masses typically range between 1.4 and 2.5 $M_{\odot}$ [1], their spectral types between AIII/V and FIII/V, and they are located inside the classical instability strip. Thanks to the *Kepler* [5,6], the *K*2 [7], the GAIA [8] and the Transiting Exoplanet Survey Satellite (TESS) [9,10] missions, as well as the All-Sky Automated Survey for Supernovae (ASAS-SN) [11] project, many studies, e.g., [12–16], based on large data sets of δ Scuti stars, have been published, providing new, tremendous knowledge for pulsators of this kind.

The eclipsing binaries (EBs) can be considered as the utmost tools for the calculation of stellar absolute parameters (e.g., masses, radii, luminosities) and the evolutionary stages of their components, particularly in cases when spectroscopy and photometry are combined. However, it should be noted that for systems with large luminosity differences between their components, the radial velocity measurements of the less luminous component are, in general, very difficult to get, because the light of the more luminous component dominates the spectrum.

In addition, given that the phase parts along the quadratures are the most important for the calculation of the amplitudes of the radial velocity curves, the systems with orbital periods longer than

1–2 days need observations in different and, depending on the orbital period, possibly distant dates. Moreover, particularly for the *Kepler* systems (with a luminosity range of approximately 10–15 mag) at least 2–4 m size telescopes have to be employed. Hence, according to these limitations, telescope time is not easy to be allocated. Therefore, for the aforementioned reasons, in the absence of radial velocity curves, the least-squares minimisation technique has to be applied to the photometric data in order to estimate the parameters of the components. Moreover, another powerful tool of the EBs is the "eclipse timing variations" (ETV) method, which allows one to detect mechanisms (e.g., mass transfer, tertiary component, etc.; c.f. Budding and Demircan [17]-ch.8 and Borkovits et al. [18] and references therein) that modulate the orbital period.

Specifically, the subject of δ Scuti stars in EBs is extremely interesting because it combines two totally different topics of astrophysics and provides the means for remarkable results. On one hand, these systems host an oscillating component, whose pulsational properties are directly measurable by analysing photometric/spectroscopic data. On the other hand, the geometric phenomena of eclipses that occur during the orbital cycles, can be used to determine the absolute properties of the components of these systems. Therefore, the study of systems of this kind, especially the detached ones with wide orbits, allows for the direct determination of the physical properties of pulsating stars. The latter can be further used to correlate their pulsation properties with their evolutionary stages, and in the future, to constrain further the current evolutionary models of the pulsating stars. Furthermore, the close detached eclipsing systems (i.e., with orbital periods in the order of a few tens of days) and the semi-detached binaries have opened a new window for examining the influences of the binarity and the mass transfer on the pulsations.

Approximately 20 years ago, Mkrtichian et al. [19] suggested the term "*oEA stars*" (oscillating eclipsing binaries of Algol type) for categorising the EBs with a δ Scuti mass accretor component of (B)A-F spectral type. A few years later, the first connection between orbital ($P_{\rm orb}$) and dominant pulsation ($P_{\rm pul}$) periods for these systems was published by Soydugan et al. [20]. Liakos et al. [21] performed a long-scale observational survey on more than 100 candidate systems, which resulted in the publication of a catalogue with 74 cases and updated correlations between fundamental parameters for these systems. The first try for a theoretical justification for the $P_{\rm pul} - P_{\rm orb}$ correlation was made by Zhang et al. [22], who derived a similar empirical relation with the previous studies, based on different assumptions (i.e., the coefficient of $\log P_{\rm orb}$ is 1), and found that its slope may be a function of the pulsation constant, the filling factor of the oscillating component and the mass ratio of the binary system. Liakos and Niarchos [23,24] announced the existence of a possible boundary in the $P_{\rm orb}$ ($\sim$13 d); beyond that $P_{\rm pul}$ and $P_{\rm orb}$ can be considered uncorrelated. Kahraman Aliçavuş et al. [25], based only on eclipsing systems, suggested an almost doubled value for this boundary. Liakos and Niarchos [26] published the most coherent catalogue for these systems to date (available online[1]), providing updated correlations between the fundamental parameters of these systems, distinguished according to geometrical status and the reliability of their absolute parameters. An extended review for binaries with pulsating components was published by Murphy [27]. Murphy et al. [28], based on a sample of 2224 *Kepler* δ Scuti light curves, employed the pulsations timing technique [29–31] and identified 341 new binaries with long $P_{\rm orb}$ ($>$ 100 d) that each host a δ Scuti component. Liakos [32], using recently discovered systems, presented updated correlations between $P_{\rm pul} - P_{\rm orb}$ and $P_{\rm pul} - \log g$ for close (i.e., $P_{\rm orb} < 13$ d) detached eclipsing binaries with δ Scuti components.

The data quality of both *Kepler* and *K*2 missions provided new insights for asteroseismology. Due to their unprecedented accuracy (i.e., order of a tens of mmag), they allow the detections of low amplitude frequencies in the order of a few μmag [33]. Moreover, the continuous data acquisition from these missions for relatively long periods of time practically extinguishes the alias effect [34] in frequency detections. The time resolution of the short-cadence data especially ($\sim$1 min) has been

[1] http://alexiosliakos.weebly.com/catalogue.html.

proven as extremely useful for the studies of short-period pulsating stars, such as the δ Scuti stars. Furthermore, the data of these missions have been widely used for the study of EBs. Specifically for the latter systems, an excellent online catalogue, namely, "*Kepler* Eclipsing Binary Catalog" (*KEBC*) [35], that is publicly available[2], has been created and includes the detrended data and other useful information for a few thousands of EBs.

The present work is a series paper on individual EBs with δ Scuti components; see also [24,32,36–40]. The system KIC 8504570 was selected for the present work because its pulsational behaviour is currently unknown to the community and its detailed analysis contributes to the sample of *Kepler*-detached binaries with a δ Scuti member (27 systems in total published to date; see Liakos and Niarchos [26] and updated lists in Liakos [32]).

KIC 8504570 (2MASS J19405685+4430276) was discovered by the *Kepler* mission [41] and has an orbital period of $\sim$4 d. The only existing references concern mostly its temperature determination at 6874–7390 K [41–48], but Davenport [49] included it in the list of *Kepler* systems that present flare activity.

Details about the ground-based spectroscopic observations and the estimation of the spectral type of the primary component of the system are given in Section 2. The *Kepler* light curve (LC) analyses, the modelling results and the absolute parameter calculations are presented in Section 3. Section 4 includes the frequency search of the LC residuals, the pulsation models and the oscillation modes' identification. Finally, Section 5 contains the summary of this work, a comparison in terms of evolution and properties of this system with other similar cases, discussion, conclusions and future prospects.

2. Spectroscopy

The purpose of the spectroscopic observations was the estimation of the spectral type of the primary component of the system. The spectra of the target were obtained with the 2.3 m Ritchey-Cretien "Aristarchos" telescope at Helmos Observatory in Greece on 6 October 2016. The *Aristarchos Transient Spectrometer*[3] (ATS) instrument [50] using the low resolution grating (600 lines mm^{-1}) was employed for the observations. This set-up provided a resolution of $\sim$3.2 Å pixel^{-1} and a spectral coverage between approximately 4000 and 7260 Å. Three successive spectra with 10 min exposures were acquired for KIC 8504570 during the orbital phase 0.81 and added together in order to achieve a better signal-to-noise ratio (S/N). The mean S/N of the individual spectra was $\sim$13, while that of the final integrated spectrum was $\sim$18. For the spectral classification, a spectral line correlation technique for the spectra of the variable and standard stars was applied. The selected standard stars, suggested by the Gemini Observatory[4], ranged between A0 and K8 spectral classes (one standard star per subclass) and were observed with the same set-up during August–October 2016. All spectra were calibrated (bias, dark, flat-field corrections) using the MaxIm DL software. The data reduction (wavelength calibration, cosmic rays removal, spectra normalisation, sky background removal) was done with the RaVeRe v.2.2c software [51].

The applied correlation method has been described in detail in Liakos [39], but is briefly presented here too. For the comparison between the spectrum of KIC 8504570 and the standard stars, the Balmer and the strong metallic lines between 4000 and 6800 Å were used. The differences of spectral line depths between each standard star and the target star were compared via sums of squared residuals in each case, with the least squares sums indicating the best fit. This method is quite efficient in cases of EBs with large luminosity differences between their components, because the total spectrum is practically dominated by the light of the primary star. In our study we did not use any synthetic spectrum approximation (c.f. [52]) in order to avoid any instrumental effects (e.g., distortion) that cannot be taken into account in a synthetic model. Therefore, using the direct comparison method,

---

[2] http://keplerebs.villanova.edu/.
[3] http://helmos.astro.noa.gr/ats.html.
[4] https://www.gemini.edu/observing/resources/near-ir-resources/spectroscopy.

and given that all spectra were acquired with the same set-up, any systematic effects were directly removed.

On the other hand, in cases with small luminosity differences between the components, this method does not provide accurate results, and more specifically, it might lead to an underestimation of the spectral type of the primary. Therefore, in order to avoid this, the following method described in [32] was applied. Using the spectra of the standard stars, all the possible combinations were calculated by simply adding and normalising the spectra. Furthermore, for every spectra combination, the spectrum of each component was given a weight between 0 and 1 denoting its light contribution to the combined spectrum. The starting value for the contribution of the primary component was 0.5 and the step was 0.05. Finally, for each spectral combination, ten sub-combinations with different light contributions of the components were derived. Similarly to the previous method, the same spectral lines were used for the comparison of the combined spectra with that of KIC 8504570, again via deriving sums of squared residuals. Hence, the smallest value of these residuals indicated again the best match.

The spectrum of KIC 8504570 was found to be dominated (at least 95%) by the light of the primary component. Therefore, its spectrum was directly compared with those of the standards. The sum of squared residuals against the spectral type for this system is plotted in Figure 1, which shows that the best fit was found with the spectrum of an A9V standard star. The spectrum of the system along with that of best-match standard star are illustrated in Figure 2. It should be noted that for the spectra continuum normalisation, polynomials of various orders were used according to the spectral types of the stars, since each spectral type has a different peak wavelength. However, for the continuum normalisation of the spectra of the standard stars with spectral types close to those of the targets (e.g., between A5–F5), the same polynomials were used. Therefore, since our method is based on direct comparison (i.e., subtraction of spectra), the non-perfect continuum normalisation does not affect the results. The present spectral classification, with an error assumption of one sub-class, corresponds to a temperature $T_{\rm eff} = 7450 \pm 150$ K for the primary, based on the relations between $T_{\rm eff}$ and spectral types of Cox [53]. The present result comes in relatively good agreement with those given in previous studies (see Section 1).

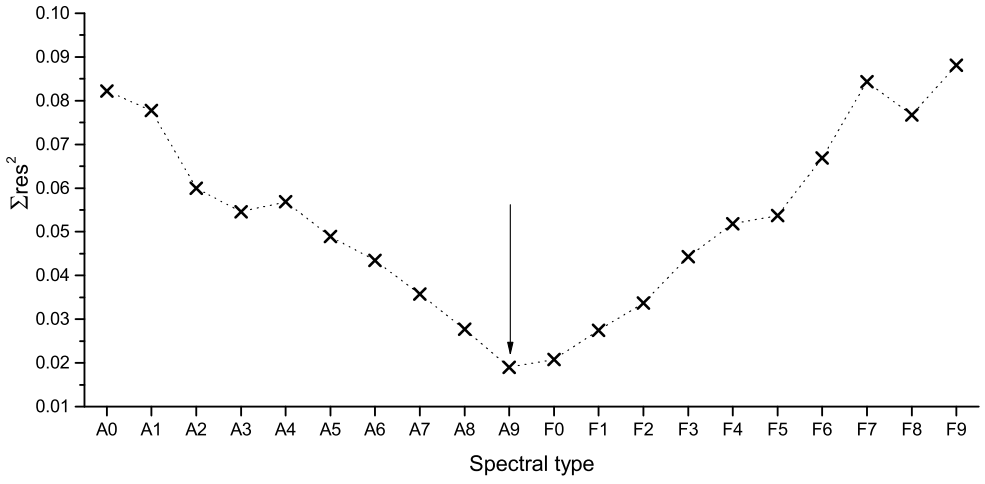

Figure 1. Spectral type-search plot for KIC 8504570. The arrow indicates the adopted spectral type for the primary component. The comparison is shown only between A0 and F9 spectral types due to scaling reasons.

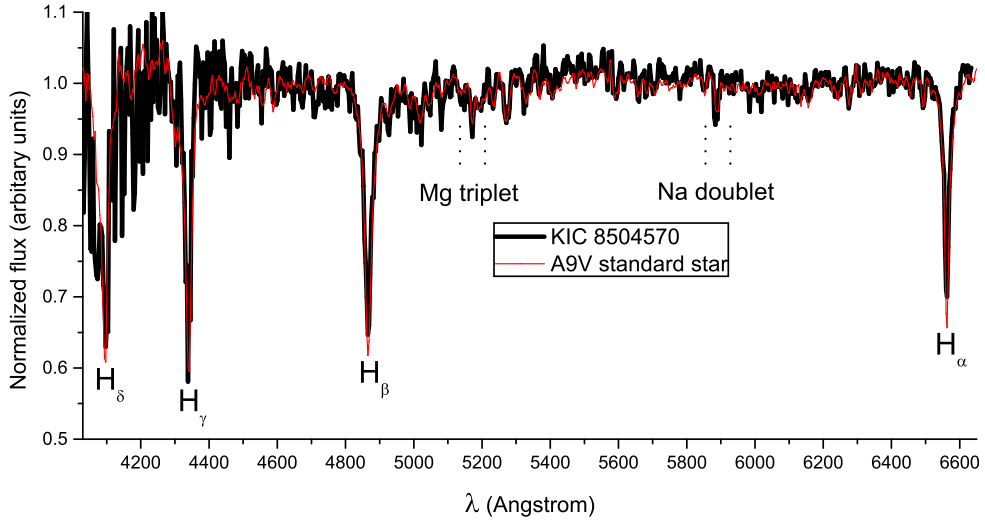

Figure 2. Comparison spectra of KIC 8504570 (black line) and the standard star (red line) with the closest spectral types. The Balmer and some strong metallic lines are also indicated.

3. Light Curve Modelling and Absolute Parameter Calculations

The system was observed in long- and short-cadence modes by the *Kepler* mission during various quarters. However, since the primary goal of this study concerns the asteroseismic analysis of the pulsating star of KIC 8504570 (i.e., pulsation modelling and mode identification), only the short-cadence data downloaded from the *KEBC* [35] were used for the frequency analysis. However, it should be noted that the data obtained for this system during non successive quarters of the *Kepler* mission provide significant time gaps, something that is crucial for the frequency analysis alias effect [34]. Furthermore, time gaps exist also within the data of a single quarter. Therefore, the selection of data for this system was made according to their continuity and total amount in time in order to include the most compact data sample possible. More specifically, the data of Q13 and a part of Q14 were selected for analysis. In total, 150,458 available points were used. These data were obtained during 106.9 consecutive days and provide 27 full LCs. The level of light contamination for this system is zero (as listed in the Mikulski Archive for Space Telescopes; MAST). The total covering and continuous time of observations is more than three months (with negligible time gaps), which is sufficient for the study of short-period pulsations and for LC modelling. The short-cadence *Kepler* LCs of the first 40 days of observations for KIC 8504570 are illustrated in Figure 3. The orbital phases and the flux to magnitude conversions for this system were derived using the ephemeris (T_0 = 2,454,955.78(3) BJD, $P_{\rm orb}$ = 4.007705(8) d) and the *Kepler* magnitude $K_{\rm p}$ = 13.25 mag, respectively, as listed in *KEBC*.

The LC analyses were done with the PHOEBE v.0.29d software [54] that is based on the 2003 version of the Wilson–Devinney code [55–57]. The temperature ($T_{\rm eff,\,1}$) of the primary component was given a value as yielded from the spectral classification (see Section 2), and it was kept fixed during the analysis. On the other hand, the temperature of the secondary component ($T_{\rm eff,\,2}$) was adjusted. The albedos (A) and the gravity darkening coefficients (g) were assigned values according to the spectral types of the components [58–60]. The (linear) limb darkening coefficients (x) were taken from the lists of van Hamme [61]. The synchronicity parameters (F) were initially adjusted, but due to the absence of significant changes during the iterations, the system was assumed to be tidally locked (i.e., $F_1 = F_2 = 1$) following the preliminary findings of Lurie et al. [62]. The dimensionless potentials (Ω), the fractional luminosity of the primary component (L_1) and the inclination of the system (i) were set as adjustable parameters. Since there is no supporting evidence for the existence of a tertiary component, and additionally, since the light contamination was zero, the third light parameter (l_3) was not taken into account. At this point, it should be noted that the R filter (Bessell photometric system—range between 550 and 870 nm and with a transmittance peak at 597 nm) simulated the best

spectral response of the CCD sensors of *Kepler* (410–910 nm with a peak at ∼588 nm). Therefore, it was used for the calculation of the filter depended parameters (i.e., x and L) in PHOEBE.

In the absence of spectroscopic mass ratio (q) for KIC 8504570, the q-search method (for details, see e.g., [63]) was applied. For this, a mean LC exempted from the presence of pulsations was needed. Moreover, in this system, except the short-period pulsations, brightness variations due to magnetic activity (e.g., spots), occurring mostly in the out-of-eclipse phase parts, were also found. Therefore, the mean LC (folded into the orbital period) was calculated from two to four successive LCs; there were no major brightness changes between them. It should be noted that a complete LC of KIC 8504570 contains approximately 5500 data points. The mean LC, using averaged points per phase, contained approximately 300 normal points, and the variations of both the pulsations and the spots almost vanished. The q-search was applied in modes 2 (detached system), 4 (semi-detached system with the primary component filling its Roche lobe) and 5 (conventional semi-detached binary) to find feasible ("photometric") estimates of the mass ratio. The step of q change during the search was 0.1 starting from $q = 0.1$. The sums of the squared residuals were systematically lower for all q values in mode 2; therefore, this system can be plausibly considered as a detached EB.

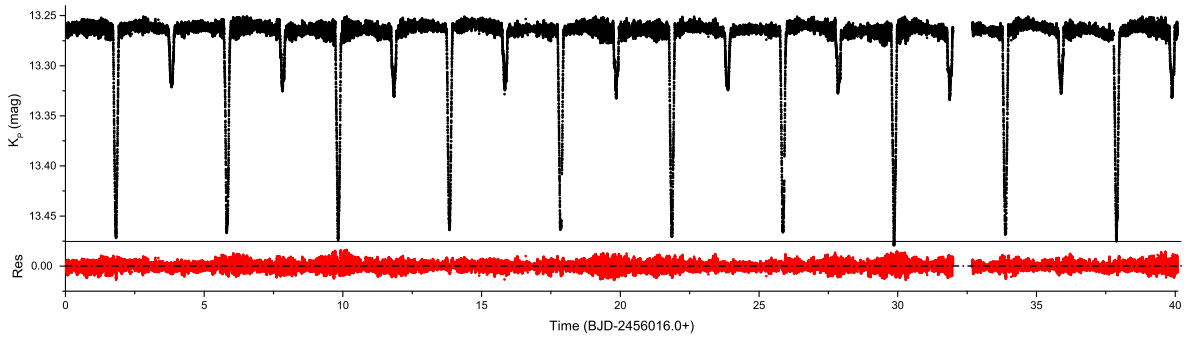

Figure 3. Short-cadence light curves (LCs) (black points) for KIC 8504570 and their residuals (red points) after the subtraction of the LC models. The plotted data concern only the first 40 days of observations, and the rest are not shown due to scaling reasons.

According to the q-search method, the minimum sum of squared residuals was found for $q = 0.5$ (Figure 4). This value was initially assigned to q, but later on it was adjusted. This system presents remarkable brightness changes from cycle to cycle after the 10 day of observations. It was found that for 40 continuous days after the 10 day, a hot spot on the surface of the secondary component describes the individual LCs very well. The selection of the hot spot was based on the results of Davenport [49] regarding possible flare activity in the system and fits well to a profile of a star with temperature of 5300 K (secondary component). Between 52 and 75 days of observations, no spots were required for the LC model, in contrast with the time range between 76 and 104 days, for which a cool spot was adopted on the surface of the same component. The spot parameters (colatitude $Colat$, longitude $long$, radius and temperature factor Tf) were adjusted in the individual LC models. Finally, for this system, one model per LC was obtained; thus, 27 models were totally derived and combined for the final average model.

The analyses of *Kepler* LCs for EBs require special handling due to light variations caused by magnetic spots between successive LCs; c.f. [32,39,40]. That justifies our choice not to model all the available points folded into the $P_{\rm orb}$, but to model each LC separately. This method provides more realistic errors for the final model results, since its single parameter (except from those of the spots) is the average from those of the individual models, while its error is the standard deviation of them. Moreover, using this method, the brightness changes due to the spots and other proximity effects are well modelled; hence, the final LC residuals can be considered as free as possible of the binarity, something that is extremely crucial for the subsequent pulsation analysis (Section 4).

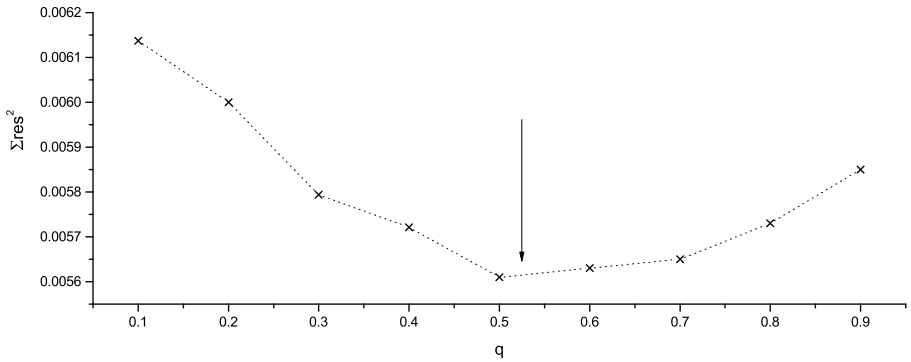

Figure 4. q-search plot for KIC 8504570. The arrow denotes the final adopted q value after the iterations.

The LCs' modelling results for KIC 8504570 are listed in Table 1. Examples of LC modelling and Roche geometry representation are plotted in Figure 5. The LC residuals after the subtraction of the individual models are illustrated below the observed LCs in Figure 3. Moreover, the parameters of the spots for each LC (cycle) are given in Table A1 in Appendix A. Figure A1 includes the immigration plots of the spots and their locations on the surface of the secondary component for two different dates of observations.

Although no RV curves exist for this system, the absolute parameters of its components can be estimated making plausible assumptions. The adopted mass (1.67 $M_{\odot}$) of the primary was based on its spectral type according to the spectral type-mass correlations of Cox [53] for main-sequence stars. A fair mass error value of 10% was also adopted. The mass of the secondary component can be directly derived from the calculated (photometric) mass ratio. The semi-major axes a can then be derived from Kepler's third law. The luminosities (L), gravity's acceleration ($\log g$) and the bolometric magnitude values ($M_{\rm bol}$) were calculated using the standard definitions. The calculations of the absolute parameters were done with the software ABSPAREB [64], and they are listed in Table 1.

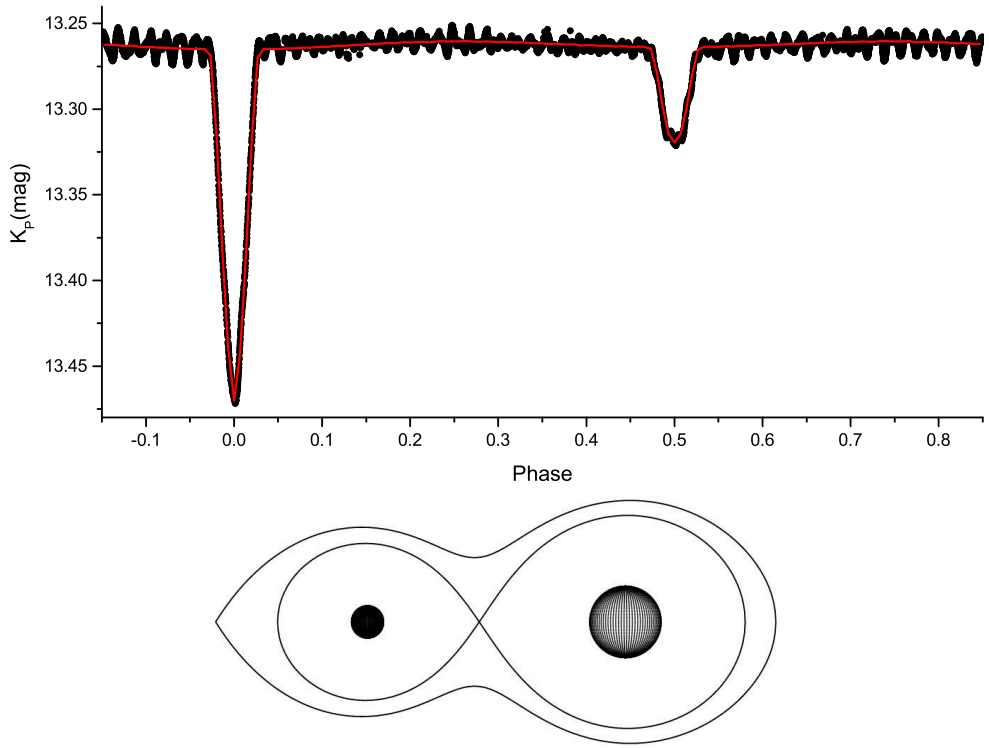

Figure 5. Example of LC modelling (solid lines) over the observed *Kepler* LCs (points) of an individual orbital cycle and the Roche geometry plot (the right star is the primary component) at orbital phase 0.75 for KIC 8504570.

Table 1. LC modelling and absolute parameters for KIC 8504570. The errors are given in parentheses alongside values and correspond to the last digit(s).

Components Parameters				Absolute Parameters	
	Primary	**Secondary**		**Primary**	**Secondary**
$T_{\rm eff}$ (K)	7450(150) [1]	5300(113)	M ($M_\odot$)	1.67(17) [a]	0.87(9)
Ω	7.76(4)	9.57(4)	R ($R_\odot$)	1.97(9)	0.89(14)
A	1 [a]	0.5 [a]	L ($L_\odot$)	11(1)	0.6(2)
g	1 [a]	0.32 [a]	$\log g$ (cm s^{-2})	4.07(5)	4.48(15)
x	0.455	0.583	a ($R_\odot$)	5.07(8)	9.75(4)
$L/L_{\rm T}$	0.945(1)	0.055(2)	$M_{\rm bol}$ (mag)	2.17(6)	5.4(2)
$r_{\rm pole}$	0.133(1)	0.060(1)		**System Parameters**	
$r_{\rm point}$	0.134(1)	0.060(1)	q (m_2/m_1)	0.52(1)	
$r_{\rm side}$	0.133(1)	0.060(1)	i (deg)	84.6(1)	
$r_{\rm back}$	0.133(1)	0.060(1)			

[1] Section 2, [a] assumed, $L_T = L_1 + L_2$.

4. Pulsation Modelling

The search for pulsation frequencies was done with the software PERIOD04 v.1.2 [65] that is based on classical Fourier analysis. Although the typical frequency range of δ Scuti stars is 4–80 d^{-1} [34], the present analysis included the regime 0–4 d^{-1} too. This selection was based on the fact that it has been noticed (e.g., [32,39]) that these stars may also exhibit longer-period oscillations due either to tidal effects, which are connected to their $P_{\rm orb}$, or even to the intrinsic hybrid behaviour of γ-Doradus–δ Scuti type. Therefore, the present pulsation analysis was done in the range 0–80 d^{-1} on the LC residuals of the system (Figure 3). Moreover, since the eclipses affect the amplitudes of the pulsations (i.e., variations of the total light) and in order to keep the data sample homogeneous, only the out-of-eclipse data were used. The ranges of orbital phases ($\Phi_{\rm orb}$) of the excluded data were 0.97–0.03 and 0.47–0.53. For the signal-to-noise ratio (S/N) calculation of the frequencies, the method for the background noise estimation, as described in detail in Liakos [39], was applied. Particularly, the background noise of the data set was calculated as 7.51 μmag in regimes with absence of frequencies, with a spacing of 2 d^{-1}, and a box size of 2. A 4σ limit (i.e.,S/N$=$ 4) [65] regarding the reliability of the detected frequencies was adopted (0.03 mmag). Hence, after the first frequency computation the residuals were subsequently pre-whitened for the next one until the detected frequency had S/N$\sim$4. The Nyquist frequency and the frequency resolution according to the Rayleigh criterion (i.e., $1/T$, where T is the observation time range in days; c.f. Aerts et al. [1], Schwarzenberg-Czerny [66]) for the present data set were 239.5 d^{-1} and 0.009 d^{-1}, respectively. According to the present spectroscopic and LC modelling results (Sections 2 and 3), only the primary component of KIC 8504570 adequately simulates the properties of δ Scuti-type stars (i.e., mass and temperature); hence, it can be plausibly concluded that this star is the pulsator of this system.

After the frequency search, the pulsation constant for each independent frequency (f) was calculated based on the relation of Breger [34]:

$$\log Q = -\log f + 0.5 \log g + 0.1 M_{\rm bol} + \log T_{\rm eff} - 6.456. \quad (1)$$

Moreover, the following pulsation constant-density relation was used for the calculation of the density of the pulsators:

$$Q = f_{\rm dom}^{-1} \sqrt{\rho_{\rm pul}/\rho_\odot}, \quad (2)$$

where $f_{\rm dom}$ is the frequency of the dominant pulsation mode (i.e., that with the largest amplitude). At this point it should be noted that the $f_{\rm dom}$ of the multiperiodic δ Scuti stars varies over time. Therefore, for a more realistic estimation of the density of this pulsator, the average value of Q of the independent frequencies was used.

The identification of the oscillating modes (i.e., l-degrees and type) employed the theoretical MAD models for δ Scuti stars [67] in the FAMIAS software v.1.01 [68]. The l-degrees from the closest MAD models (i.e., f, $\log g$, M and $T_{\rm eff}$) to the detected independent frequencies were adopted as the most possible pulsation modes. Moreover, the ratio $P_{\rm pul}/P_{\rm orb}$ of all independent frequencies was calculated in order to check whether it is less than 0.07, which is the upper value, according to Zhang et al. [22], for the discrimination of p-type modes.

Table 2 includes the pulsation modelling results regarding the independent frequencies for KIC 8504570 as well as their respective mode identification. Particularly, this table lists: The frequency value $f_{\rm i}$, the amplitude A, the phase Φ, the S/N, the Q, the $P_{\rm pul}/P_{\rm orb}$, the l-degrees and the mode of each detected independent frequency. The rest of the detected frequencies (i.e., dependent/combination frequencies) are given in Appendix B (Table A2). Figure 6 shows the periodogram of the pulsating star of KIC 8504570 and the distribution of its oscillation frequencies. Representative Fourier fittings on the LC residuals are plotted in Figure 7.

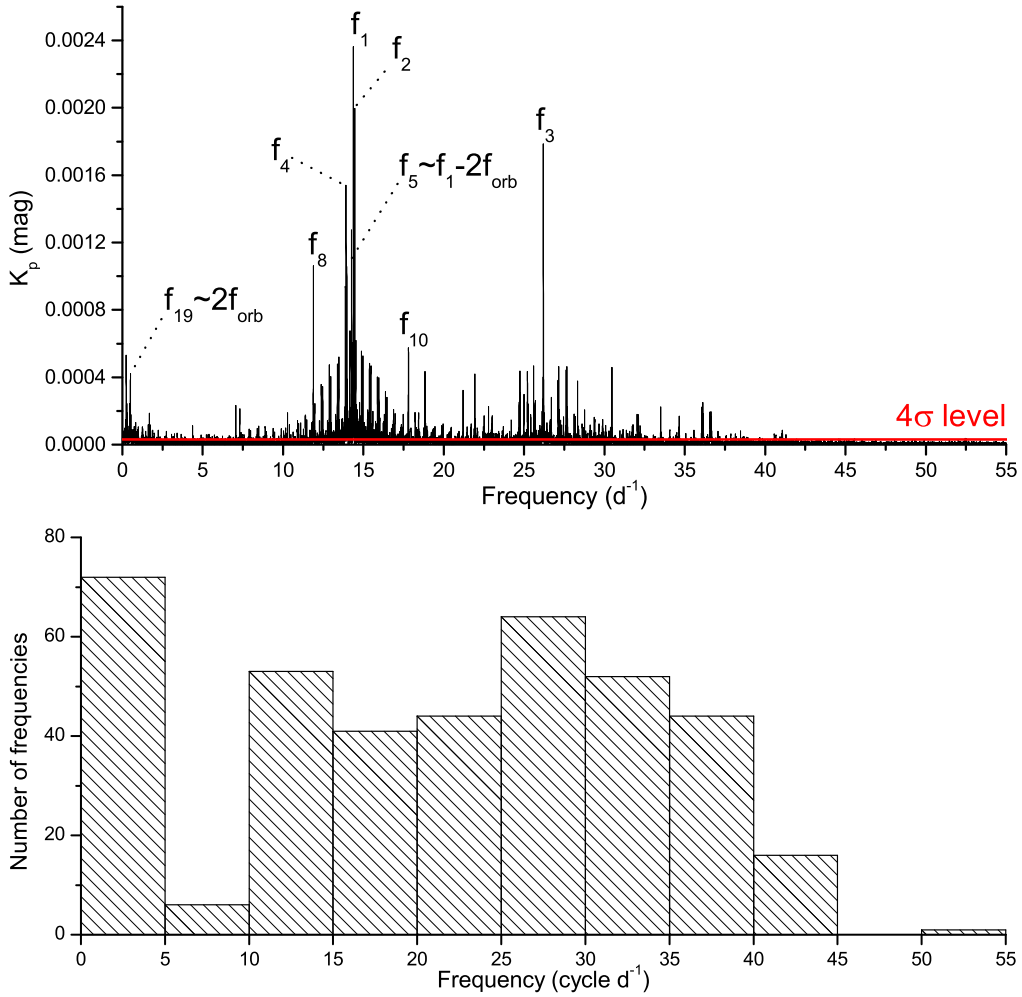

Figure 6. Periodogram (**top**) and frequency distribution (**bottom**) for KIC 8504570. The independent frequencies, the strong frequencies that are connected to the $P_{\rm orb}$ and the significance level are also indicated.

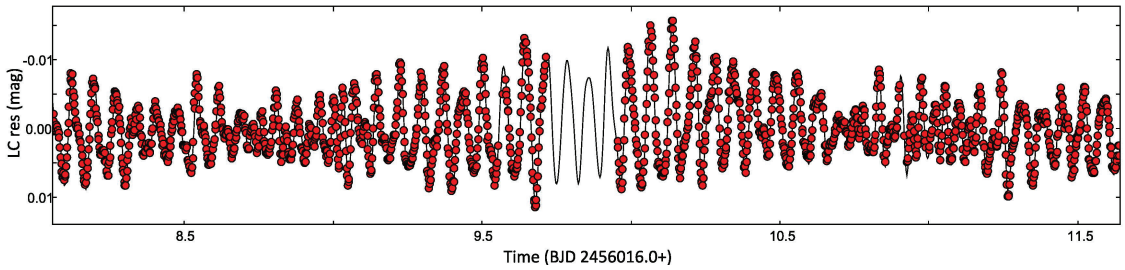

Figure 7. Representative example of Fourier fitting (solid line) on various data points for KIC 8504570.

Table 2. Frequency search results and mode identification for the independent frequencies of the pulsating component of KIC 8504570. The errors are given in parentheses alongside values and correspond to the last digit(s).

i	f_i (d^{-1})	A (mmag)	Φ (°)	S/N	Q (d)	P_{pul}/P_{orb} [1]	l-Degree	Pulsation Mode
1	14.37417(1)	2.550(5)	1.8(1)	339.3	0.032(2)	0.017	3 or 1	NR p
2	14.46668(1)	2.215(5)	59.2(1)	294.7	0.032(2)	0.017	1 or 3	NR p
3	26.19524(1)	1.779(5)	32.1(1)	236.7	0.018(1)	0.010	2	NR p
4	13.91847(2)	1.560(5)	236.5(2)	207.6	0.033(2)	0.018	2 or 3	NR p
8	11.89034(2)	1.070(5)	57.1(2)	142.4	0.039(2)	0.021	3	NR p
10	17.80685(4)	0.565(5)	264.1(5)	75.2	0.026(2)	0.014	1	NR p

[1] Error values are of 10^{-7}–10^{-8} order of magnitude. NR p non-radial pressure mode.

The pulsator of KIC 8504570 oscillates in a total of 393 frequencies. Six of them are independent and were detected in the regime 11.8–26.2 d^{-1}. Among the other 387 depended frequencies, 309 were spread almost uniformly in the range 10–43.4 d^{-1}; 72 had values less than 4.4 d^{-1}; five were found between 5.5–9 d^{-1}; and only one, namely, f_{282}, exceeded 50 d^{-1}. As can be seen in Figure 6, one main concentration of frequencies is between 12 and 17 d^{-1}, while a slightly more spread out one is between 23 and 30 d^{-1}. The results based on MAD models show that all oscillations are probably non-radial pressure modes. Although the ratio f_4/f_{10} has value ∼0.78, f_4 was not identified as a radial mode by the MAD models. Finally, a value of ρ_{pul} = 0.215(4) $\rho_\odot$ was derived.

5. Summary, Discussion and Conclusions

In the present work, detailed LC and pulsation modellings for KIC 8504570, a neglected *Kepler*-detached EB with an oscillating component, are presented. The spectral classification of its primary component, based on our spectroscopic observations, provided the means for accurate LC analyses, and for the estimation of the absolute parameters and evolutionary stages of both the components of the EB. The primary component was also identified as a δ Scuti star and its pulsational characteristics (pulsation frequencies model and mode identification) were accurately determined.

The primary component of KIC 8504570 was classified as an A9-type star and pulsates in six independent frequencies in the regime 11.89–26.2 d^{-1} with the dominant part at 14.37 d^{-1}. These frequencies were identified as non-radial (pressure) modes according to the MAD models. Moreover, this star oscillates in another 387 combination frequencies. During the LC modelling, initially a hot and subsequently a cool spot on the surface of the secondary component were used to overcome the brightness asymmetries in the quadratures. This selection can be justified from the fact that this EB was listed as a possible flare system [49].

For the estimation of the evolutionary stages of the components of KIC 8504570, the locations of its members on the mass-radius ($M-R$) and Hertzsprung–Russell (HR) diagrams are illustrated in Figures 8 and 9, respectively. Both components are located inside the main-sequence and follow the theoretical evolutionary tracks of Girardi et al. [69] (see Figure 9) very well according to their derived masses and the corresponding error ranges (see Table 1). Therefore, it seems that they have been

evolving without any significant interactions so far. In terms of evolution, the δ Scuti component of KIC 8504570 has similar absolute properties to other δ Scuti stars in detached binary systems. It is among the eight less massive and less luminous stars of this sample and it is located closer to red edge of the classical instability strip.

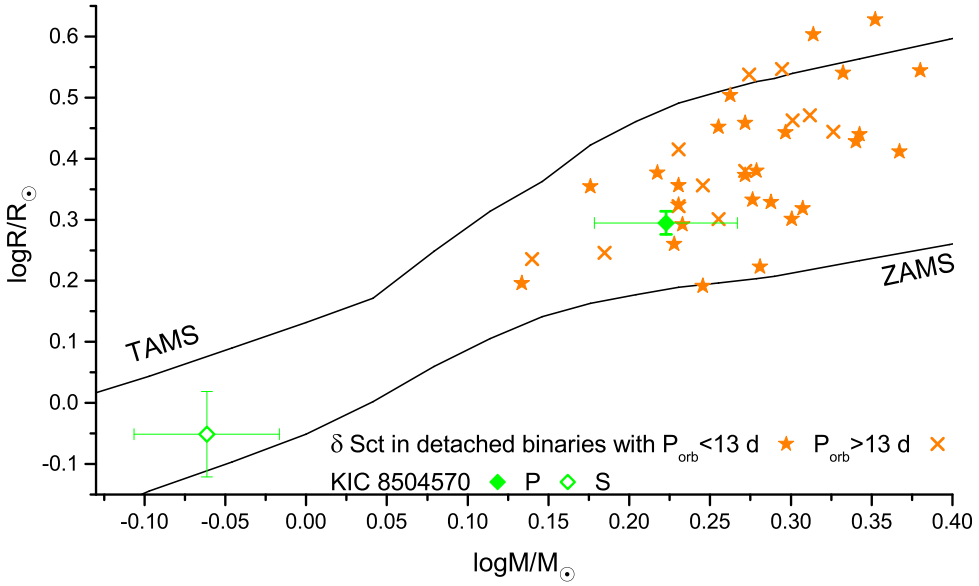

Figure 8. Locations of the primary (filled symbol) and secondary (empty symbol) components of KIC 8504570 (diamonds) within the mass-radius diagram. The stars and the "×" symbols denote the δ Scuti components of other detached systems with $P_{\rm orb}$ shorter and longer than 13 d, respectively (taken from Liakos and Niarchos [26] and Liakos [32]). The black solid lines represent the main-sequence edges.

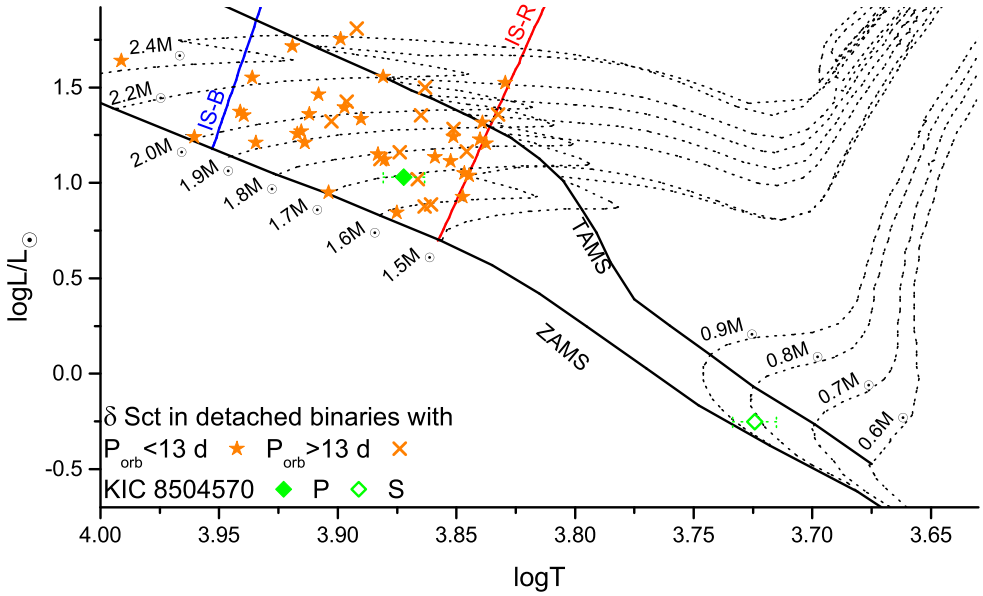

Figure 9. Locations of the components of KIC 8504570 within the *HR* diagram. Symbols and black solid lines have the same meanings as in Figure 8. Dotted lines denote the evolutionary tracks for stars with masses between 0.6–0.9 $M_{\odot}$ and 1.5–2.4 $M_{\odot}$ (taken from Girardi et al. [69]) and the coloured solid lines (B = blue, R = red) indicate the boundaries of the instability strip (IS; taken from Soydugan et al. [70]).

In order to check the accordance of the pulsational properties of the δ Scuti star of KIC 8504570 with others that belong in similar systems, it was placed on the $P_{\rm pul} - P_{\rm orb}$ and $\log g - P_{\rm pul}$ diagrams

(Figures 10 and 11, respectively) along with the well established empirical relations of Liakos [32] for δ Scuti stars in detached binaries with $P_{\rm orb} < 13$ d. The studied star in these plots follows very well both the distributions of the sample stars and the empirical relations.

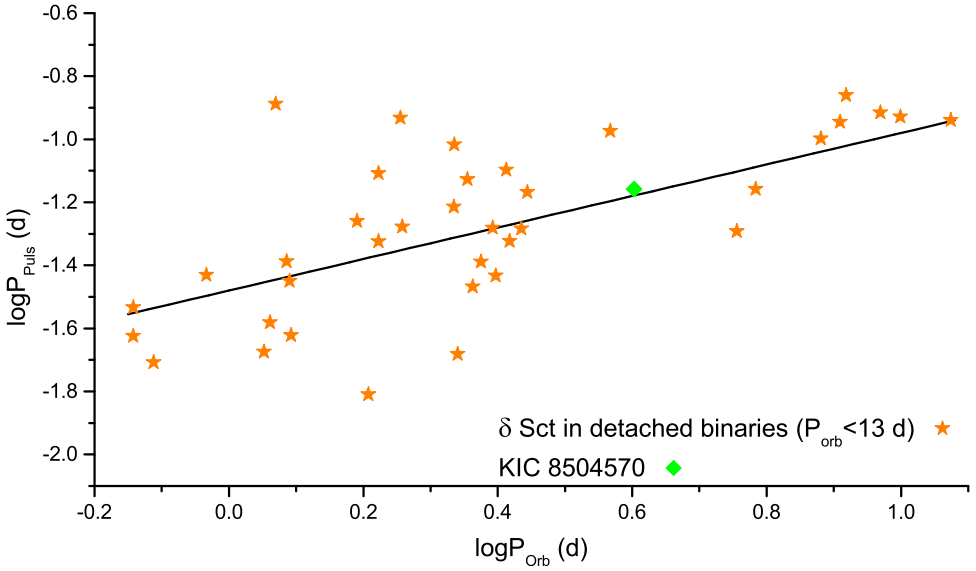

Figure 10. Location of the oscillating (primary) component of KIC 8504570 among other δ Scuti stars-members of detached systems with $P_{\rm orb} < 13$ d within the $P_{\rm orb} - P_{\rm pul}$ diagram. Symbols have the same meanings as in Figure 8, while the solid line denotes the empirical linear fit of Liakos [32].

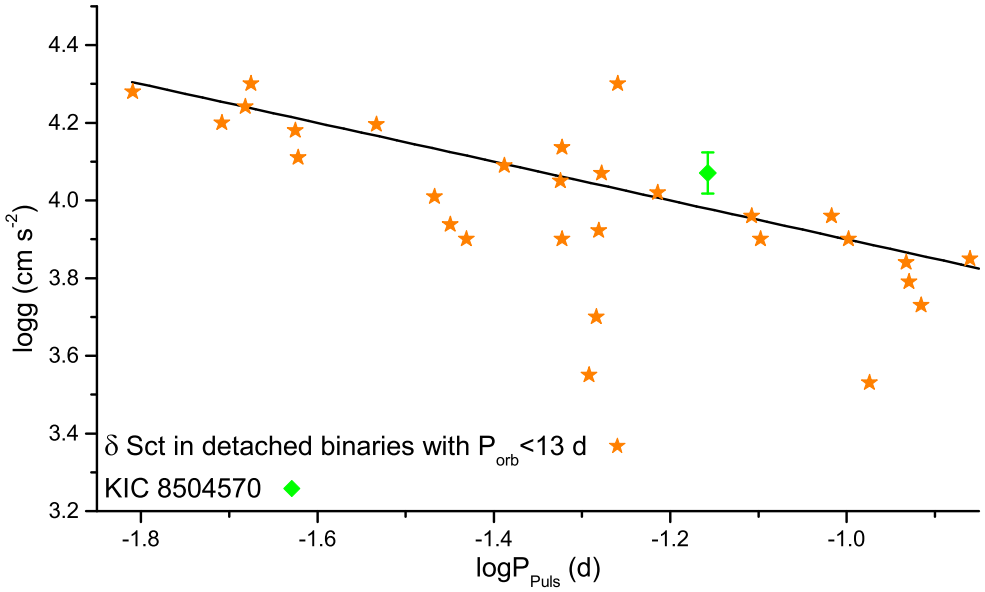

Figure 11. Location of the δ Scuti (primary) star of KIC 8504570 within the $\log g - P_{\rm pul}$ diagram. Symbols and lines have the same meanings as in Figure 10.

Using the current dominant oscillation frequency of the pulsator and the pulsation period-luminosity relation for δ Scuti stars of Ziaali et al. [14],

$$M_{\rm V} = -2.94(6) \log P_{\rm pul} - 1.34(6), \quad (3)$$

it is feasible to calculate its absolute magnitude ($M_{\rm V} = 2.06(13)$ mag). Hence, using the apparent magnitude ($m_{\rm V}$) and the distance modulus, its distance can be calculated. The $m_{\rm V}$ of KIC 8504570 is 13.28 mag according to the NOMAD-1 catalogue [71] and the extinction in V band is $A_{\rm V} = 0.336$ mag [47];

thus, its distance is determined as 1502^{+93}_{-87} pc. This value is in very good agreement with the value 1488 ± 41 pc. as derived by Berger et al. [47] and Bailer-Jones et al. [72], and in slight disagreement with the value 1305 pc of Queiroz et al. [73]. The latter discrepancy is attributed to the different extinction value ($A_V = 0.474$ mag) used by Queiroz et al. [73]. It should be noted that the aforementioned M_V is in very good agreement with the $M_{bol,1}$ = 2.17(6) mag, which was calculated based on the LC model;ing (Table 1).

For the future, radial velocity measurements are welcome to validate the present results for the LC model, although the ∼95% light domination of the primary component makes the acquisition of the radial velocities of the secondary an extremely difficult task. At best, we anticipate that only the radial velocities of the primary can be measured, which will only constrain the mass of the primary component, and hence the mass ratio of the system. However, these potential future measurements cannot significantly change the present pulsations models, especially the results for the dominant and the independent frequencies, which were the main goals of the present study. The asteroseismic modelling of other similar systems, especially of those observed by satellite missions, is highly encouraged and recommended because the sample of δ Scuti stars in binary systems is still small and we lack of enough information. Moreover, systems with P_{orb} between 10 and 20 d should be prioritised for detailed analysis in order to check the reasons for the existence of the boundary of $P_{orb} \sim 13$ d.

Author Contributions: A.L.: Observations, data reduction and analysis, writing; P.N.: General review and consultation. All authors have read and agreed to the published version of the manuscript.

Funding: This research was funded by the European Space Agency (ESA) under the Near Earth object Lunar Impacts and Optical TrAnsients (NELIOTA) programme, contract number 4000112943.

Acknowledgments: The authors wish to thank Mrs Maria Pizga for proofreading the text and the three anonymous reviewers for their fruitful comments. The "Aristarchos" telescope is operated on Helmos Observatory by the Institute for Astronomy, Astrophysics, Space Applications and Remote Sensing of the National Observatory of Athens. This research has made use of NASA's Astrophysics Data System Bibliographic Services, the SIMBAD, the Mikulski Archive for Space Telescopes (MAST) and the *Kepler* Eclipsing Binary Catalog data bases.

Conflicts of Interest: The authors declare no conflict of interest.

Abbreviations

The following abbreviations are used in this manuscript:

BJD	Barycentric Julian date
EB	Eclipsing binary system
ETV	Eclipse timing variations
KEBC	Kepler Eelipsing binary catalogue
KIC	Kepler input catalogue
LC	Light curve

Appendix A. Spot Migration

This appendix includes information for the variation of the spots locations in time, which were assumed to be located on the surface of the secondary part of the system (see also Section 3). It should be noted that the present solution is just a suggestion for describing the LC asymmetries in the quadratures, and more solutions (e.g., more spots with different sizes and temperatures) may result in the same LC behaviour (degeneracy of solutions). The average BJD values of the points included in the models from which the respective parameters (colatitude *Colat.*, longitude *long.*, radius and temperature factor Tf) were calculated, were set as corresponding timings for each cycle in Table A1. The upper part of Figure A1 shows the changes of the parameters of all spots over time for the system, and the lower parts show the spot(s) on the secondary part's surface during different days of observations.

Table A1. Spot parameters for KIC 8504570.

Time (BJD 2456016.0+)	Colat. (°)	long. (°)	Radius (°)	Tf ($\frac{T_{spot}}{T_{eff}}$)	Time (BJD 2456016.0+)	Colat. (°)	long. (°)	Radius (°)	Tf ($\frac{T_{spot}}{T_{eff}}$)
12.04	90(6)	140(6)	10(2)	1.18(5)	52.12	74(6)	78(6)	11(2)	1.09(4)
16.05	90(5)	147(5)	10(1)	1.25(2)	76.16	83(2)	20(4)	14(1)	0.81(6)
20.05	90(6)	135(6)	10(2)	1.25(4)	80.17	83(2)	16(1)	14(1)	0.72(12)
24.06	73(5)	131(5)	12(1)	1.24(2)	84.18	83(1)	13(2)	14(1)	0.69(16)
28.07	73(5)	126(5)	12(1)	1.24(3)	88.19	73(2)	13(2)	14(1)	0.65(11)
32.69	75(3)	122(2)	12(1)	1.27(4)	92.19	73(1)	13(2)	14(1)	0.64(11)
36.08	77(1)	107(3)	12(1)	1.25(4)	96.20	73(4)	2(4)	14(4)	0.57(8)
40.09	75(2)	99(3)	12(1)	1.22(5)	100.21	69(3)	−12(2)	15(3)	0.77(5)
44.10	73(9)	87(5)	12(1)	1.17(4)	104.22	68(5)	−13(5)	14(5)	0.76(11)
48.11	73(8)	75(7)	13(1)	1.17(2)					

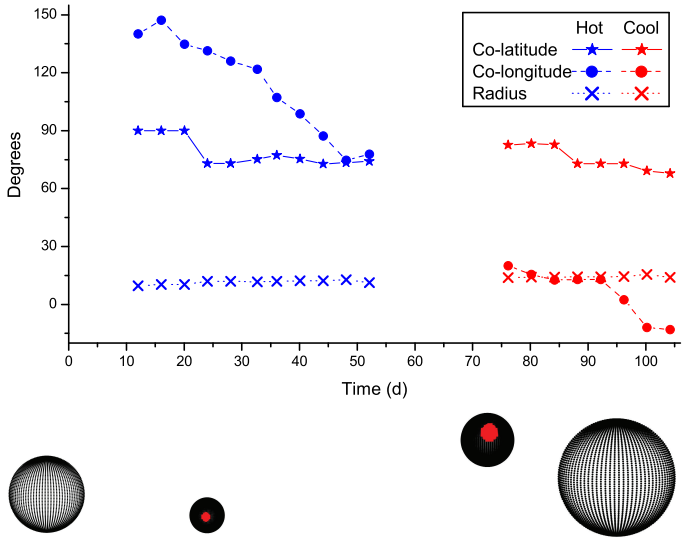

Figure A1. Top panel: Spot migration diagram for KIC 8504570. Lower left panel shows the hot spot on the surface of the secondary at orbital phase 0.10 during the 12th day, and the lower right panel illustrates the cool spot on the same component at an orbital phase of 0.55 during the 104th day of observations.

Appendix B. Combination Frequencies

Table A2 contains the values of the depended frequencies f_i (where i is an increasing number), semi-amplitudes A, phases Φ and S/N for KIC 8504570. Moreover, in the last column of this table, the most likely combination for each frequency is also given. The combinations were calculated only for the first 255 frequencies because this is the maximum number of frequencies that the software can detect during one run (i.e., Fourier model). However, it should be noted that in order to continue the search, the residuals from these Fourier models were given as new data sets to the same software, but no combinations could be calculated using the first 255 frequencies.

Table A2. Combination frequencies of KIC 8504570.

i	f_i (d^{-1})	A (mmag)	Φ (°)	S/N	Combination	i	f_i (d^{-1})	A (mmag)	Φ (°)	S/N	Combination
5	13.96772(2)	1.462(5)	25.8(2)	194.5	$f_1 - 2f_{orb}$	44	15.81073(12)	0.195(5)	172.1(1.3)	26	$f_2 + f_{39} - f_4$
6	14.26173(2)	1.197(5)	127.1(2)	159.2	$f_1 + 2f_4 - 2f_5$	45	0.46827(12)	0.193(5)	315.2(1.4)	25.7	$2f_{12}$
7	13.87519(2)	1.187(5)	304.5(2)	158	$f_1 + f_5 - f_2$	46	14.30447(12)	0.191(5)	262.1(1.4)	25.4	$f_3 - f_8$
9	14.15746(4)	0.620(5)	84.7(4)	82.6	$f_1 + f_6 - f_2$	47	18.43246(13)	0.190(5)	331.8(1.4)	25.3	$f_{18} + f_5 - f_1$
11	14.52475(4)	0.556(5)	315.2(5)	74	$f_2 + f_5 - f_4$	48	18.21829(13)	0.188(5)	159.1(1.4)	25	$f_{37} - f_{39}$
12	0.23719(4)	0.539(5)	127.8(5)	71.7	$f_9 - f_4$	49	10.27324(13)	0.184(5)	131.9(1.4)	24.5	$f_{21} - f_2$
13	25.59738(5)	0.467(5)	196.9(6)	62.1	$f_3 + f_7 - f_2$	50	25.41796(13)	0.180(5)	185.4(1.5)	23.9	$f_2 + f_{22} - f_6$
14	27.16046(5)	0.469(5)	134.7(6)	62.3	$3f_7 - f_2$	51	13.41866(14)	0.176(5)	265.4(1.5)	23.4	$f_4 - 2f_{orb}$
15	30.46276(5)	0.464(5)	153.0(6)	61.7	$f_{11} + 2f_4 - f_8$	52	0.28509(14)	0.175(5)	333.8(1.5)	23.3	$f_6 - f_5$
16	27.61182(5)	0.517(5)	4.5(5)	68.9	$f_1 + f_{14} - f_4$	53	32.03430(14)	0.173(5)	177.3(1.5)	23	$f_{21} + f_{41}$
17	27.11303(5)	0.462(5)	323.8(6)	61.5	$f_{16} + f_5 - f_2$	54	1.67956(14)	0.169(5)	153.5(1.6)	22.5	$f_4 + f_5 - f_3$
18	18.83497(5)	0.441(5)	315.3(6)	58.7	$f_{15} + f_5 - f_{13}$	55	36.13223(14)	0.166(5)	97.7(1.6)	22.1	$\sim f_{31}$
19	0.49692(6)	0.388(5)	245.8(7)	51.6	$2f_{orb}$	56	34.65322(14)	0.166(5)	239.4(1.6)	22.2	$f_{25} + f_{28}$
20	21.93578(6)	0.411(5)	94.0(6)	54.7	$2f_3 - f_{15}$	57	32.10851(14)	0.167(5)	152.4(1.6)	22.2	$f_{10} + f_{46}$
21	24.73787(6)	0.409(5)	44.4(6)	54.4	$f_{17} + f_8 - f_6$	58	22.50879(14)	0.166(5)	266.8(1.6)	22.1	$f_{34} - f_{52}$
22	25.20896(6)	0.402(5)	29.2(7)	53.5	$f_{13} + f_7 - f_6$	59	36.09231(15)	0.163(5)	251.8(1.6)	21.7	$f_{20} + f_9$
23	27.65926(6)	0.386(5)	351.2(7)	51.4	$f_{14} + 2f_{orb}$	60	12.96918(15)	0.162(5)	42.6(1.6)	21.5	$f_{17} - f_9$
24	28.33090(6)	0.370(5)	248.9(7)	49.2	$f_1 + f_5$	61	27.46012(15)	0.162(5)	65.2(1.6)	21.5	$f_{40} + f_{60}$
25	13.44778(7)	0.354(5)	305.5(7)	47.1	$f_{16} - f_9$	62	15.58199(15)	0.161(5)	230.0(1.6)	21.4	$f_{61} - f_8$
26	24.70969(7)	0.347(5)	0.6(8)	46.1	$f_{22} - 2f_{orb}$	63	29.89821(15)	0.160(5)	223.4(1.7)	21.2	$f_{46} + f_{62}$
27	13.99402(7)	0.341(5)	100.8(8)	45.3	$f_1 + f_7 - f_6$	64	13.69577(15)	0.157(5)	334.2(1.7)	20.9	$f_{16} - f_4$
28	21.19886(8)	0.306(5)	75.1(9)	40.7	$f_{18} + f_6 - f_8$	65	29.36747(15)	0.155(5)	212.2(1.7)	20.7	$f_{42} + f_8$
29	24.98915(8)	0.284(5)	211.7(9)	37.8	$f_{22} + f_9 - f_1$	66	0.26866(16)	0.152(5)	22.9(1.7)	20.3	$\sim f_{orb}$
30	17.78666(9)	0.276(5)	127.0(1.0)	36.7	$f_{10} + f_5 - f_{27}$	67	36.62210(16)	0.152(5)	336.5(1.7)	20.3	$f_{21} + f_8$
31	36.12330(10)	0.240(5)	139.7(1.1)	32	$f_3 + f_{29} - f_2$	68	25.23620(16)	0.148(5)	271.9(1.8)	19.7	$f_{21} + 2f_{orb}$
32	36.06506(10)	0.232(5)	18.6(1.1)	30.8	$f_1 + f_{20} - f_{12}$	69	1.75471(17)	0.143(5)	195.6(1.8)	19	$7f_{orb}$
33	7.06065(10)	0.231(5)	274.2(1.1)	30.7	$f_1 + f_7 - f_{28}$	70	23.00711(17)	0.138(5)	131.6(1.9)	18.4	$f_{58} + 2f_{orb}$
34	22.78777(10)	0.229(5)	349.1(1.1)	30.5	$f_1 + f_3 - f_{30}$	71	14.60554(17)	0.137(5)	235.0(1.9)	18.2	$2f_{41}$
35	36.56292(10)	0.228(5)	75.9(1.2)	30.3	$2f_{orb} + f_{32}$	72	0.24564(18)	0.135(5)	61.3(1.9)	18	$\sim f_{12}$
36	0.48424(11)	0.227(5)	125.2(1.2)	30.2	$\sim 2f_{orb}$	73	14.41579(18)	0.135(5)	140.8(1.9)	18	$f_4 + 2f_{orb}$
37	33.50439(11)	0.223(5)	66.3(1.2)	29.7	$f_1 + f_3 - f_{33}$	74	30.07058(18)	0.135(5)	341.8(2.0)	17.9	$f_{44} + f_6$
38	28.75971(11)	0.219(5)	74.6(1.2)	29.1	$2f_1$	75	36.59298(18)	0.132(5)	243.6(2.0)	17.5	$f_{26} + f_8$
39	15.27483(11)	0.212(5)	334.8(1.2)	28.2	$f_{14} - f_8$	76	36.14820(18)	0.133(5)	101.8(2.0)	17.7	$f_{67} - f_{36}$

Table A2. *Cont.*

i	f_i (d^{-1})	A (mmag)	Φ (°)	S/N	Combination	i	f_i (d^{-1})	A (mmag)	Φ (°)	S/N	Combination
40	14.49281(12)	0.206(5)	320.2(1.3)	27.4	$f_{12} + f_6$	77	1.61146(19)	0.129(5)	94.4(2.0)	17.1	$f_{62} - f_5$
41	7.30582(12)	0.202(5)	98.9(1.3)	26.9	$f_1 - f_{33}$	78	11.09517(18)	0.130(5)	327.0(2.0)	17.3	$f_{13} - f_{40}$
42	17.46822(12)	0.199(5)	106.4(1.3)	26.5	$f_{10} + f_4 - f_6$	79	29.86627(19)	0.129(5)	249.8(2.0)	17.1	$f_{65} + 2f_{orb}$
43	0.25832(12)	0.199(5)	80.8(1.3)	26.4	f_{orb}	80	29.39894(19)	0.128(5)	19.2(2.1)	17	$f_{63} - 2f_{orb}$
81	29.65398(19)	0.128(5)	5.7(2.1)	17	$f_1 + f_{39}$	118	1.88387(27)	0.088(5)	75.6(3.0)	11.7	$f_{44} - f_4$
82	0.50819(19)	0.127(5)	319.2(2.1)	16.9	$\sim 2f_{orb}$	119	23.64493(27)	0.088(5)	357.2(3.0)	11.7	$f_{67} - f_{60}$
83	13.62955(19)	0.125(5)	139.7(2.1)	16.6	$f_7 - f_{12}$	120	23.41808(27)	0.087(5)	79.5(3.0)	11.6	$f_{119} - f_{12}$
84	31.77175(20)	0.122(5)	241.8(2.2)	16.2	$f_{10} + f_5$	121	0.59273(27)	0.087(5)	226.5(3.0)	11.5	$f_2 - f_7$
85	26.41931(20)	0.121(5)	35.6(2.2)	16.1	$f_{12} + f_3$	122	0.45887(27)	0.088(5)	318.0(3.0)	11.7	$\sim f_{45}$
86	16.23344(20)	0.119(5)	170.1(2.2)	15.8	$f_2 + f_{69}$	123	0.21840(27)	0.088(5)	216.5(3.0)	11.7	$f_2 - f_6$
87	0.82146(20)	0.117(5)	183.8(2.2)	15.6	$f_{39} - f_2$	124	27.10128(28)	0.086(5)	248.2(3.1)	11.5	$\sim f_{17}$
88	13.94799(20)	0.117(5)	250.4(2.3)	15.6	$f_{24} - f_1$	125	0.03147(28)	0.086(5)	239.7(3.1)	11.4	$f_4 - f_7$
89	27.26003(20)	0.117(5)	220.8(2.3)	15.6	$2f_{83}$	126	0.14043(28)	0.087(5)	63.0(3.0)	11.5	$f_{11} - f_1$
90	16.75243(21)	0.116(5)	61.5(2.3)	15.4	$f_{53} - f_{39}$	127	34.64194(28)	0.086(5)	264.6(3.1)	11.4	$\sim f_{56}$
91	15.05783(21)	0.113(5)	108.8(2.3)	15.1	$f_{25} + f_{77}$	128	0.94076(28)	0.084(5)	79.9(3.1)	11.2	$2f_{45}$
92	0.52933(21)	0.113(5)	141.6(2.3)	15.1	$2f_{orb}$	129	36.05708(28)	0.084(5)	156.5(3.1)	11.2	$\sim f_{32}$
93	0.34709(21)	0.112(5)	44.7(2.3)	15	$f_6 - f_4$	130	10.15488(29)	0.083(5)	350.0(3.2)	11.1	$f_{16} - f_{42}$
94	18.74761(21)	0.111(5)	155.5(2.4)	14.8	$f_{35} - f_{10}$	131	18.94535(29)	0.083(5)	120.1(3.2)	11.1	$f_{33} + f_8$
95	36.63478(22)	0.108(5)	271.3(2.4)	14.4	$\sim f_{67}$	132	31.73511(29)	0.083(5)	308.6(3.2)	11	$f_{10} + f_4$
96	12.27641(22)	0.109(5)	16.7(2.4)	14.4	$f_3 - f_4$	133	0.73974(29)	0.082(5)	202.6(3.2)	11	$f_1 - f_{83}$
97	22.96202(22)	0.106(5)	296.7(2.5)	14.1	$f_{26} - f_{69}$	134	16.30624(30)	0.080(5)	50.4(3.3)	10.7	$f_{15} - f_9$
98	22.46229(22)	0.109(5)	292.1(2.4)	14.5	$f_{67} - f_9$	135	16.02725(30)	0.080(5)	134.9(3.3)	10.7	$f_{63} - f_7$
99	21.69765(23)	0.105(5)	288.0(2.5)	13.9	$f_{32} - f_1$	136	31.16305(30)	0.080(5)	85.4(3.3)	10.6	$2f_{62}$
100	4.37269(23)	0.103(5)	131.4(2.5)	13.8	$f_{18} - f_2$	137	12.97670(30)	0.080(5)	177.2(3.3)	10.6	$\sim f_{60}$
101	21.88975(24)	0.101(5)	143.3(2.6)	13.4	$f_{76} - f_6$	138	0.99431(30)	0.080(5)	127.4(3.3)	10.6	$4f_{orb}$
102	13.65820(24)	0.100(5)	55.8(2.6)	13.3	$f_4 - f_{orb}$	139	27.62122(30)	0.079(5)	208.7(3.3)	10.6	$\sim f_{16}$
103	36.64746(24)	0.099(5)	305.0(2.7)	13.2	$\sim f_{95}$	140	10.03276(30)	0.079(5)	321.0(3.3)	10.5	$f_{20} - f_8$
104	27.34082(24)	0.099(5)	147.9(2.7)	13.1	$f_1 + f_{60}$	141	38.46793(31)	0.078(5)	45.6(3.4)	10.3	$f_3 + f_{96}$
105	26.63865(24)	0.099(5)	96.3(2.6)	13.2	$f_1 + f_{96}$	142	36.07352(31)	0.078(5)	157.9(3.4)	10.3	$\sim f_{32}$
106	32.23532(25)	0.097(5)	127.1(2.7)	12.9	$f_{10} + f_{73}$	143	21.94752(31)	0.078(5)	0.3(3.4)	10.3	$\sim f_{20}$
107	36.11673(25)	0.097(5)	107.4(2.7)	12.9	$\sim f_{31}$	144	26.66871(31)	0.077(5)	44.1(3.4)	10.3	$f_3 + f_{36}$
108	36.57325(25)	0.096(5)	208.1(2.7)	12.8	$\sim f_{35}$	145	18.99466(31)	0.076(5)	169.6(3.5)	10.1	$f_{12} + f_{94}$
109	32.22593(25)	0.095(5)	65.5(2.8)	12.6	$\sim f_{106}$	146	13.85546(31)	0.076(5)	39.8(3.5)	10.1	$f_{24} - f_2$
110	12.35531(25)	0.095(5)	281.4(2.8)	12.6	$f_{45} + f_8$	147	14.35473(31)	0.078(5)	76.3(3.4)	10.4	$f_{24} - f_5$
111	0.47672(25)	0.094(5)	33.8(2.8)	12.5	$\sim f_{36}$	148	21.47033(32)	0.075(5)	150.6(3.5)	10	$f_{41} + f_9$
112	11.69260(26)	0.092(5)	19.3(2.9)	12.2	$f_{13} - f_4$	149	26.14173(32)	0.076(5)	14.0(3.5)	10.1	$f_6 + f_8$

Table A2. *Cont.*

i	$f_{\rm i}$ ($\rm d^{-1}$)	A (mmag)	Φ (°)	S/N	Combination	i	$f_{\rm i}$ ($\rm d^{-1}$)	A (mmag)	Φ (°)	S/N	Combination
113	21.44966(26)	0.092(5)	127.2(2.9)	12.2	$f_{12} + f_{28}$	150	25.03236(32)	0.075(5)	283.6(3.5)	9.9	$f_{21} + f_{52}$
114	36.55494(26)	0.091(5)	211.4(2.9)	12.1	$\sim f_{35}$	151	28.36237(32)	0.074(5)	211.9(3.5)	9.9	$f_1 + f_{27}$
115	22.08279(26)	0.090(5)	140.7(2.9)	12	$f_{35} - f_2$	152	21.67229(32)	0.074(5)	20.0(3.6)	9.9	$f_{41} + f_1$
116	29.08191(27)	0.089(5)	203.6(2.9)	11.9	$f_{71} + f_2$	153	10.95004(32)	0.074(5)	127.8(3.6)	9.8	$f_{22} - f_6$
117	30.36789(27)	0.089(5)	120.1(2.9)	11.9	$f_{79} + 2f_{\rm orb}$	154	31.12219(33)	0.072(5)	30.7(3.6)	9.6	$f_1 + f_{90}$
155	0.72753(33)	0.072(5)	11.2(3.6)	9.6	$\sim f_{133}$	192	40.56879(40)	0.060(5)	122.9(4.4)	7.9	$f_3 + f_1$
156	17.96654(33)	0.072(5)	292.0(3.7)	9.6	$f_{79} - f_8$	193	23.34011(40)	0.059(5)	104.6(4.4)	7.9	$f_{163} - f_{11}$
157	31.72666(33)	0.072(5)	225.9(3.7)	9.5	$\sim f_{132}$	194	24.53309(40)	0.059(5)	54.8(4.5)	7.8	$f_{49} + f_6$
158	31.36642(33)	0.072(5)	21.3(3.7)	9.6	$f_2 + f_{154}$	195	0.74773(41)	0.059(5)	131.1(4.5)	7.8	$\sim f_{133}$
159	26.18870(34)	0.071(5)	52.9(3.7)	9.4	$\sim f_3$	196	1.98861(41)	0.058(5)	212.3(4.5)	7.7	$f_7 - f_8$
160	41.07370(34)	0.070(5)	250.4(3.8)	9.3	$f_{14} + f_4$	197	14.38056(41)	0.058(5)	183.0(4.5)	7.7	$\sim f_1$
161	16.77450(34)	0.069(5)	135.3(3.8)	9.2	$f_{15} - f_{64}$	198	41.29397(41)	0.058(5)	78.0(4.6)	7.7	$f_{80} + f_8$
162	33.51284(35)	0.069(5)	163.5(3.8)	9.2	$\sim f_{37}$	199	0.06059(42)	0.057(5)	1.5(4.6)	7.6	$f_5 - f_4$
163	37.86299(35)	0.069(5)	171.6(3.8)	9.1	$f_{13} + f_{96}$	200	13.73006(42)	0.057(5)	265.5(4.7)	7.5	$f_5 - f_{12}$
164	36.10311(35)	0.068(5)	194.3(3.9)	9.1	$\sim f_{59}$	201	25.09952(42)	0.056(5)	142.7(4.7)	7.5	$f_{13} - 2f_{\rm orb}$
165	37.85124(35)	0.068(5)	324.1(3.9)	9	$\sim f_{163}$	202	27.83304(42)	0.057(5)	192.4(4.7)	7.5	$2f_4$
166	36.03547(36)	0.067(5)	275.4(3.9)	8.9	$f_1 + f_{152}$	203	0.21229(43)	0.056(5)	71.7(4.7)	7.4	$\sim f_{123}$
167	36.53427(34)	0.070(5)	313.3(3.8)	9.3	$f_{71} + f_{20}$	204	13.37545(44)	0.055(5)	311.6(4.8)	7.3	$f_7 - 2f_{\rm orb}$
168	27.15624(36)	0.067(5)	43.3(3.9)	8.9	$\sim f_{14}$	205	27.87061(44)	0.055(5)	247.7(4.8)	7.3	$f_7 + f_{27}$
169	27.71186(36)	0.066(5)	241.6(4.0)	8.8	$2f_{146}$	206	36.62821(44)	0.055(5)	312.0(4.8)	7.3	$\sim f_{67}$
170	27.60008(36)	0.066(5)	276.2(4.0)	8.8	$\sim f_{16}$	207	40.66602(44)	0.054(5)	243.5(4.9)	7.2	$f_3 + f_2$
171	18.39489(36)	0.066(5)	195.7(4.0)	8.8	$f_{10} + f_{121}$	208	32.08314(44)	0.054(5)	324.2(4.9)	7.2	$f_7 + f_{48}$
172	0.12212(36)	0.066(5)	320.6(4.0)	8.8	$f_1 - f_6$	209	34.06565(43)	0.055(5)	166.9(4.8)	7.3	$f_{56} + f_{121}$
173	26.16757(37)	0.065(5)	250.0(4.0)	8.7	$f_2 + f_{112}$	210	0.53590(44)	0.054(5)	260.0(4.9)	7.1	$\sim f_{92}$
174	0.16955(37)	0.065(5)	161.0(4.1)	8.6	$f_2 - f_{46}$	211	13.27118(45)	0.054(5)	98.1(4.9)	7.1	$f_{23} - f_1$
175	1.45412(37)	0.064(5)	238.5(4.1)	8.6	$f_3 - f_{21}$	212	36.65545(45)	0.053(5)	295.0(4.9)	7.1	$\sim f_{103}$
176	34.00412(37)	0.064(5)	68.4(4.1)	8.5	$2f_{\rm orb} + f_{37}$	213	19.21306(45)	0.053(5)	121.4(4.9)	7.1	$f_{37} - f_{46}$
177	14.17625(38)	0.063(5)	215.8(4.2)	8.4	$f_2 - f_{52}$	214	17.64669(45)	0.053(5)	359.8(5.0)	7.0	$f_{53} - f_1$
178	31.61018(38)	0.063(5)	119.0(4.2)	8.4	$2f_{44}$	215	24.26679(45)	0.053(5)	326.2(5.2)	7.0	$f_{76} - f_8$
179	31.57402(37)	0.064(5)	155.1(4.1)	8.6	$f_{53} - f_{45}$	216	0.90554(46)	0.052(5)	216.3(5.1)	6.9	$f_{17} - f_3$
180	0.20196(38)	0.063(5)	242.0(4.2)	8.4	$f_2 - f_6$	217	18.97682(46)	0.052(5)	3.4(5.1)	6.9	$f_{37} - f_{11}$
181	0.29824(34)	0.070(5)	324.0(3.8)	9.3	$\sim f_{52}$	218	25.70775(46)	0.052(5)	220.8(5.1)	6.9	$f_3 - 2f_{\rm orb}$
182	18.49634(38)	0.062(5)	290.9(4.2)	8.3	$f_{18} - f_{93}$	219	41.04270(46)	0.052(5)	92.9(5.1)	6.9	$f_{17} + f_4$
183	25.20520(38)	0.062(5)	94.1(4.2)	8.3	$\sim f_{22}$	220	0.08877(46)	0.052(5)	110.0(5.1)	6.9	$f_2 - f_1$
184	28.10451(39)	0.062(5)	305.5(4.3)	8.2	$f_2 + f_{83}$	221	3.05619(46)	0.052(5)	32.8(5.1)	6.9	$f_{29} - f_{20}$
185	30.26831(39)	0.062(5)	199.9(4.3)	8.2	$f_2 + f_{44}$	222	14.02595(46)	0.051(5)	47.5(5.1)	6.8	$f_6 - f_{12}$
186	16.08924(39)	0.062(5)	146.7(4.3)	8.2	$f_{15} - f_1$	223	10.47896(47)	0.051(5)	73.4(5.2)	6.8	$f_{21} - f_6$

Table A2. *Cont.*

i	f_i (d^{-1})	A (mmag)	Φ (°)	S/N	Combination	i	f_i (d^{-1})	A (mmag)	Φ (°)	S/N	Combination
187	3.65737(39)	0.061(5)	46.8(4.3)	8.2	$f_{10} - f_9$	224	30.62339(47)	0.051(5)	314.4(5.2)	6.8	$f_7 + f_{90}$
188	3.40985(38)	0.062(5)	305.7(4.3)	8.2	$f_{30} - f_1$	225	22.68914(47)	0.051(5)	177.7(5.2)	6.8	$f_{35} - f_7$
189	17.81296(39)	0.061(5)	136.4(4.3)	8.2	$\sim f_{10}$	226	7.57260(47)	0.051(5)	39.1(5.2)	6.7	$f_{20} - f_1$
190	28.39102(40)	0.060(5)	214.7(4.4)	8	$f_2 + f_4$	227	38.64171(47)	0.050(5)	98.2(5.2)	6.7	$f_{26} + f_{41}$
191	34.45924(40)	0.060(5)	2.7(4.4)	7.9	$f_{14} + f_{41}$	228	38.14057(42)	0.057(5)	102.1(4.7)	7.5	$f_{215} + f_7$
229	1.59878(48)	0.050(5)	8.5(5.3)	6.7	$\sim f_{77}$	266	23.07991(50)	0.043(4)	337.3(5.5)	5.7	
230	27.08297(48)	0.050(5)	107.0(5.3)	6.6	$f_{219} - f_5$	267	32.05825(50)	0.042(4)	235.4(5.6)	5.6	
231	0.70827(48)	0.049(5)	220.6(5.3)	6.6	$f_1 - f_{102}$	268	38.92399(50)	0.042(4)	157.0(5.6)	5.6	
232	34.62597(49)	0.048(5)	111.9(5.4)	6.5	$f_{51} + f_{28}$	269	13.99214(50)	0.042(4)	310.0(5.6)	5.6	
233	0.38842(49)	0.048(5)	314.4(5.4)	6.4	$f_6 - f_7$	270	31.07569(51)	0.042(4)	107.8(5.6)	5.6	
234	15.59984(49)	0.048(5)	73.3(5.5)	6.4	$f_{74} - f_2$	271	31.39131(50)	0.042(4)	171.7(5.6)	5.6	
235	40.92481(50)	0.048(5)	116.2(5.5)	6.4	$f_6 + f_{144}$	272	0.12822(51)	0.042(4)	86.1(5.6)	5.6	
236	24.74257(50)	0.048(5)	157.2(5.5)	6.4	$\sim f_{21}$	273	18.60718(51)	0.042(4)	318.8(5.6)	5.6	
237	0.19398(50)	0.047(5)	117.9(5.6)	6.3	$\sim f_{180}$	274	18.47614(50)	0.042(4)	353.0(5.6)	5.6	
238	26.20326(50)	0.047(5)	297.0(5.6)	6.3	$\sim f_3$	275	40.52840(51)	0.042(4)	229.9(5.6)	5.6	
239	0.83696(51)	0.047(5)	323.3(5.6)	6.3	$f_2 - f_{83}$	276	18.33665(51)	0.042(4)	287.7(5.7)	5.5	
240	0.86374(49)	0.049(5)	336.6(5.4)	6.5	$f_{13} - f_{21}$	277	11.47702(51)	0.042(4)	147.2(5.7)	5.5	
241	28.33935(51)	0.047(5)	186.2(5.6)	6.3	$\sim f_{24}$	278	26.46018(51)	0.041(4)	1.4(5.7)	5.5	
242	30.09078(51)	0.047(5)	216.2(5.6)	6.2	$f_{12} - f_{79}$	279	21.75167(52)	0.041(4)	3.4(5.7)	5.5	
243	36.37364(51)	0.047(5)	196.1(5.6)	6.2	$f_{58} + f_7$	280	14.12834(52)	0.041(4)	1.5(5.7)	5.5	
244	27.16892(51)	0.047(5)	218.8(5.6)	6.2	$\sim f_{14}$	281	27.27976(52)	0.041(4)	6.7(5.7)	5.5	
245	22.59802(51)	0.047(5)	183.6(5.6)	6.2	$f_{35} - f_5$	282	52.44645(52)	0.041(4)	116.8(5.8)	5.4	
246	41.05115(51)	0.046(5)	38.3(5.7)	6.2	$\sim f_{129}$	283	18.66448(53)	0.040(4)	330.3(5.8)	5.4	
247	0.01738(52)	0.046(5)	358.1(5.7)	6.1	$f_{27} - f_5$	284	32.63830(53)	0.040(4)	272.2(5.8)	5.4	
248	18.44796(52)	0.046(5)	233.8(5.7)	6.1	$f_{48} + f_{12}$	285	32.26773(53)	0.040(4)	144.4(5.8)	5.4	
249	28.88230(53)	0.045(5)	324.7(5.8)	6	$f_2 + f_{73}$	286	32.13246(53)	0.040(4)	58.5(5.8)	5.4	
250	11.91476(53)	0.045(5)	207.0(5.8)	6	$f_{125} + f_8$	287	27.88330(53)	0.040(4)	75.1(5.9)	5.3	
251	1.22304(53)	0.045(5)	218.1(5.9)	5.9	$f_{24} - f_{17}$	288	38.65768(53)	0.040(4)	300.7(5.9)	5.3	
252	25.08167(54)	0.044(5)	194.0(5.9)	5.9	$f_{13} - f_{82}$	289	17.62462(53)	0.040(4)	300.3(5.9)	5.3	
253	18.41978(54)	0.044(5)	313.2(6.0)	5.8	$\sim f_{47}$	290	34.28546(54)	0.040(4)	70.5(5.9)	5.3	
254	0.41942(55)	0.044(5)	215.3(6.0)	5.8	$f_1 - f_5$	291	0.57676(54)	0.040(4)	267.5(5.9)	5.3	
255	38.19834(55)	0.044(5)	200.8(6.1)	5.8	$f_{21} + f_{25}$	292	3.91476(53)	0.040(4)	24.5(5.9)	5.3	
256	37.87661(49)	0.044(4)	247.1(5.4)	5.8		293	0.18176(53)	0.040(4)	152.7(5.9)	5.3	
257	31.67828(49)	0.043(4)	206.9(5.4)	5.8		294	40.69514(54)	0.040(4)	323.4(5.9)	5.3	
258	40.59838(49)	0.043(4)	304.0(5.5)	5.7		295	29.56990(54)	0.039(4)	136.9(6.0)	5.2	
259	21.17303(50)	0.043(4)	3.0(5.5)	5.7		296	30.29039(54)	0.039(4)	163.6(6.0)	5.3	

Table A2. *Cont.*

i	f_i (d^{-1})	A (mmag)	Φ (°)	S/N	Combination	i	f_i (d^{-1})	A (mmag)	Φ (°)	S/N	Combination
260	0.78389(50)	0.043(4)	350.5(5.5)	5.7		297	27.21213(54)	0.039(4)	178.6(6.0)	5.2	
261	2.67105(50)	0.043(4)	252.9(5.5)	5.7		298	0.98303(54)	0.039(4)	338.9(6.0)	5.2	
262	5.59244(50)	0.043(4)	217.8(5.5)	5.7		299	36.43047(55)	0.039(4)	346.3(6.0)	5.2	
263	14.36553(50)	0.043(4)	343.9(5.5)	5.7		300	36.04909(54)	0.039(4)	220.3(6.0)	5.2	
264	26.13140(50)	0.042(4)	308.0(5.5)	5.6		301	0.49504(55)	0.039(4)	284.1(6.1)	5.1	
265	22.87795(50)	0.042(4)	136.7(5.6)	5.6		302	22.02925(55)	0.039(4)	249.9(6.1)	5.1	
303	22.84977(56)	0.038(4)	22.1(6.1)	5.1		340	2.33640(61)	0.035(4)	201.6(6.8)	4.6	
304	38.82301(56)	0.038(4)	84.4(6.2)	5.1		341	5.79546(61)	0.035(4)	323.3(6.8)	4.6	
305	36.08432(56)	0.038(4)	328.8(6.2)	5		342	8.99316(61)	0.035(4)	94.4(6.8)	4.6	
306	17.28880(56)	0.038(4)	138.2(6.2)	5		343	40.57713(62)	0.035(4)	49.3(6.8)	4.6	
307	32.83745(56)	0.038(4)	283.2(6.2)	5		344	23.28876(62)	0.034(4)	153.6(6.8)	4.6	
308	0.44478(57)	0.038(4)	112.8(6.3)	5		345	32.32647(62)	0.034(4)	311.9(6.8)	4.6	
309	0.40909(56)	0.038(4)	131.4(6.2)	5		346	38.62485(62)	0.034(4)	117.6(6.9)	4.5	
310	20.29755(57)	0.038(4)	256.7(6.3)	5		347	43.33923(62)	0.034(4)	325.0(6.9)	4.5	
311	25.51472(57)	0.037(4)	349.6(6.3)	5		348	26.17857(62)	0.034(4)	65.6(6.9)	4.5	
312	34.44515(57)	0.037(4)	134.3(6.3)	5		349	24.85296(63)	0.034(4)	62.6(6.9)	4.5	
313	31.94882(55)	0.038(4)	28.5(6.1)	5.1		350	1.30086(63)	0.034(4)	146.9(6.9)	4.5	
314	34.08021(57)	0.038(4)	81.9(6.3)	5		351	12.47697(63)	0.034(4)	175.2(7.0)	4.5	
315	22.79623(57)	0.037(4)	283.8(6.3)	5		352	22.24233(63)	0.034(4)	97.3(7.0)	4.5	
316	13.47549(57)	0.037(4)	269.2(6.3)	4.9		353	13.96989(63)	0.034(4)	350.7(7.0)	4.5	
317	15.35138(57)	0.037(4)	198.7(6.3)	4.9		354	0.11682(63)	0.034(4)	172.3(7.0)	4.5	
318	26.50339(58)	0.037(4)	159.5(6.4)	4.9		355	38.84400(63)	0.034(4)	299.6(7.0)	4.5	
319	14.42471(58)	0.037(4)	356.5(6.4)	4.9		356	36.01940(63)	0.034(4)	304.2(7.0)	4.5	
320	18.24741(58)	0.037(4)	328.3(6.4)	4.9		357	0.37396(63)	0.034(4)	180.4(7.0)	4.5	
321	17.79464(58)	0.037(4)	332.9(6.4)	4.9		358	41.03200(63)	0.034(4)	135.0(7.0)	4.5	
322	40.93702(58)	0.037(4)	93.1(6.4)	4.9		359	26.21200(64)	0.033(4)	43.0(7.1)	4.4	
323	33.49546(58)	0.037(4)	10.4(6.4)	4.9		360	28.15600(64)	0.033(4)	352.1(7.1)	4.4	
324	13.92591(58)	0.037(4)	272.1(6.4)	4.9		361	32.02800(64)	0.033(4)	214.8(7.1)	4.4	
325	13.95691(56)	0.038(4)	4.9(6.2)	5.1		362	23.12800(64)	0.033(4)	277.8(7.1)	4.4	
326	12.96200(57)	0.038(4)	205.9(6.2)	5		363	23.19200(63)	0.034(4)	310.8(7.0)	4.5	
327	3.99150(58)	0.036(4)	29.1(6.5)	4.8		364	1.20800(64)	0.033(4)	27.0(7.1)	4.4	
328	25.99003(59)	0.036(4)	39.2(6.5)	4.8		365	0.80800(64)	0.033(4)	326.9(7.1)	4.4	
329	32.17410(58)	0.036(4)	314.5(6.5)	4.8		366	15.02400(64)	0.033(4)	183.1(7.1)	4.4	
330	0.65755(59)	0.036(4)	164.6(6.5)	4.8		367	23.75200(65)	0.033(4)	63.5(7.1)	4.4	
331	37.96485(59)	0.036(4)	288.9(6.5)	4.8		368	30.63200(65)	0.033(4)	44.7(7.2)	4.4	
332	40.99194(60)	0.036(4)	219.8(6.6)	4.8		369	22.22400(66)	0.032(4)	57.2(7.3)	4.3	

Table A2. *Cont.*

i	f_i (d^{-1})	A (mmag)	Φ (°)	S/N	Combination	i	f_i (d^{-1})	A (mmag)	Φ (°)	S/N	Combination
333	16.60626(60)	0.035(4)	150.4(6.6)	4.7		370	0.16000(66)	0.032(4)	22.5(7.3)	4.3	
334	18.21105(61)	0.035(4)	45.2(6.7)	4.7		371	25.36400(67)	0.032(4)	286.6(7.4)	4.2	
335	36.66564(61)	0.035(4)	256.7(6.7)	4.6		372	32.10000(67)	0.032(4)	114.0(7.4)	4.2	
336	38.35755(61)	0.035(4)	267.6(6.7)	4.6		373	0.07200(67)	0.032(4)	258.4(7.4)	4.2	
337	32.37003(60)	0.036(4)	13.3(6.6)	4.7		374	30.66400(67)	0.032(4)	223.7(7.5)	4.2	
338	36.54486(61)	0.035(4)	273.7(6.7)	4.6		375	30.15200(67)	0.032(4)	227.3(7.4)	4.2	
339	38.19024(61)	0.035(4)	288.6(6.8)	4.6		376	36.58400(68)	0.031(4)	146.9(7.5)	4.2	
377	21.98800(68)	0.031(4)	337.6(7.5)	4.2		386	27.12000(69)	0.031(4)	155.5(7.7)	4.1	
378	0.60400(68)	0.031(4)	199.3(7.6)	4.1		387	26.86800(68)	0.031(4)	150.9(7.6)	4.1	
379	24.72800(68)	0.031(4)	174.4(7.6)	4.1		388	26.76000(68)	0.031(4)	31.3(7.5)	4.2	
380	11.54800(69)	0.031(4)	139.7(7.6)	4.1		389	40.55200(70)	0.030(4)	165.7(7.8)	4.0	
381	12.04400(68)	0.031(4)	251.3(7.5)	4.2		390	33.04000(70)	0.030(4)	245.9(7.7)	4.0	
382	31.75600(68)	0.031(4)	5.6(7.6)	4.1		391	26.03200(70)	0.030(4)	307.6(7.8)	4.0	
383	22.86000(69)	0.031(4)	263.6(7.6)	4.1		392	30.45600(71)	0.030(4)	253.3(7.8)	4.0	
384	24.38800(69)	0.031(4)	210.8(7.6)	4.1		393	27.76000(71)	0.030(4)	47.3(7.8)	4.0	
385	38.91200(69)	0.031(4)	195.7(7.7)	4.1							

References

1. Aerts, C.; Christensen-Dalsgaard, J.; Kurtz, D.W. *Asteroseismology*; Springer: Dordrecht, The Netherlands, 2010. [CrossRef]
2. Balona, L.A.; Daszyńska-Daszkiewicz, J.; Pamyatnykh, A.A. Pulsation frequency distribution in δ Scuti stars. *Mon. Not. R. Astron. Soc.* **2015**, *452*, 3073–3084. [CrossRef]
3. Antoci, V.; Cunha, M.; Houdek, G.; Kjeldsen, H.; Trampedach, R.; Handler, G.; Lüftinger, T.; Arentoft, T.; Murphy, S. The Role of Turbulent Pressure as a Coherent Pulsational Driving Mechanism: The Case of the δ Scuti Star HD 187547. *Astrophys. J.* **2014**, *796*, 118. [CrossRef]
4. Grassitelli, L.; Fossati, L.; Langer, N.; Miglio, A.; Istrate, A.G.; Sanyal, D. Relating turbulent pressure and macroturbulence across the HR diagram with a possible link to γ Doradus stars. *Astron. Astrophys.* **2015**, *584*, L2. [CrossRef]
5. Borucki, W.J.; Koch, D.; Basri, G.; Batalha, N.; Brown, T.; Caldwell, D.; Caldwell, J.; Christensen-Dalsgaard, J.; Cochran, W.D.; DeVore, E.; et al. Kepler Planet-Detection Mission: Introduction and First Results. *Science* **2010**, *327*, 977–980. [CrossRef] [PubMed]
6. Koch, D.G.; Borucki, W.J.; Basri, G.; Batalha, N.M.; Brown, T.M.; Caldwell, D.; Christensen-Dalsgaard, J.; Cochran, W.D.; DeVore, E.; Dunham, E.W.; et al. Kepler Mission Design, Realized Photometric Performance, and Early Science. *Astrophys. J.* **2010**, *713*, L79–L86. [CrossRef]
7. Howell, S.B.; Sobeck, C.; Haas, M.; Still, M.; Barclay, T.; Mullally, F.; Troeltzsch, J.; Aigrain, S.; Bryson, S.T.; Caldwell, D.; et al. The K2 Mission: Characterization and Early Results. *Publ. Astron. Soc. Pac.* **2014**, *126*, 398. [CrossRef]
8. Gaia Collaboration; Prusti, T.; de Bruijne, J.H.J.; Brown, A.G.A.; Vallenari, A.; Babusiaux, C.; Bailer-Jones, C.A.L.; Bastian, U.; Biermann, M.; Evans, D.W.; et al. The Gaia mission. *Astron. Astrophys.* **2016**, *595*, A1. [CrossRef]
9. Ricker, G.R.; Latham, D.W.; Vanderspek, R.K.; Ennico, K.A.; Bakos, G.; Brown, T.M.; Burgasser, A.J.; Charbonneau, D.; Deming, L.D.; Doty, J.P.; et al. *The Transiting Exoplanet Survey Satellite (TESS)*; American Astronomical Society Meeting Abstracts, American Astronomical Society Meeting #213; American Astronomical Society: Long Beach, CA, USA; 2009; Volume 214, p. 306.5.
10. Ricker, G.R.; Winn, J.N.; Vanderspek, R.; Latham, D.W.; Bakos, G.Á.; Bean, J.L.; Berta-Thompson, Z.K.; Brown, T.M.; Buchhave, L.; Butler, N.R.; et al. Transiting Exoplanet Survey Satellite (TESS). *J. Astron. Telesc. Instrum. Syst.* **2015**, *1*, 014003. [CrossRef]
11. Shappee, B.; Prieto, J.; Stanek, K.Z.; Kochanek, C.S.; Holoien, T.; Jencson, J.; Basu, U.; Beacom, J.F.; Szczygiel, D.; Pojmanski, G.; et al. *All Sky Automated Survey for SuperNovae (ASAS-SN or "Assassin")*; American Astronomical Society Meeting Abstracts, American Astronomical Society Meeting #223; American Astronomical Society: Washington, DC, USA; 2014; Volume 223, p. 236.03.
12. Bowman, D.M.; Kurtz, D.W. Characterizing the observational properties of δ Sct stars in the era of space photometry from the Kepler mission. *Mon. Not. R. Astron. Soc.* **2018**, *476*, 3169–3184. [CrossRef]
13. Murphy, S.J.; Hey, D.; Van Reeth, T.; Bedding, T.R. Gaia-derived luminosities of Kepler A/F stars and the pulsator fraction across the δ Scuti instability strip. *Mon. Not. R. Astron. Soc.* **2019**, *485*, 2380–2400. [CrossRef]
14. Ziaali, E.; Bedding, T.R.; Murphy, S.J.; Van Reeth, T.; Hey, D.R. The period-luminosity relation for δ Scuti stars using Gaia DR2 parallaxes. *Mon. Not. R. Astron. Soc.* **2019**, *486*, 4348–4353. [CrossRef]
15. Bedding, T.R.; Murphy, S.J.; Hey, D.R.; Huber, D.; Li, T.; Smalley, B. Stello, D.; White, T.R.; Ball, W.H.; Chaplin, W.J.; et al. Very regular high-frequency pulsation modes in young intermediate-mass stars. *Nature* **2020**, *581*, 147–151. [CrossRef] [PubMed]
16. Jayasinghe, T.; Stanek, K.Z.; Kochanek, C.S.; Vallely, P.J.; Shappee, B.J.; Holoien, T.W.S.; Thompson, T.A.; Prieto, J.L.; Pejcha, O.; Fausnaugh, M.; et al. The ASAS-SN catalogue of variable stars VI: An all-sky sample of δ Scuti stars. *Mon. Not. R. Astron. Soc.* **2020**, *493*, 4186–4208. [CrossRef]
17. Budding, E.; Demircan, O. *Introduction to Astronomical Photometry*; Cambridge University Press: New York, NY, USA, 2007. [CrossRef]
18. Borkovits, T.; Hajdu, T.; Sztakovics, J.; Rappaport, S.; Levine, A.; Bíró, I.B.; Klagyivik, P. A comprehensive study of the Kepler triples via eclipse timing. *Mon. Not. R. Astron. Soc.* **2016**, *455*, 4136–4165. [CrossRef]

19. Mkrtichian, D.E.; Kusakin, A.V.; Gamarova, A.Y.; Nazarenko, V. Pulsating Components of Eclipsing Binaries: New Asteroseismic Methods of Studies and Prospects. In *International Astronomical Union Colloquium 185: Radial and Nonradial Pulsationsn as Probes of Stellar Physics Leuven, Belgium, 26–31 July 2002;* Aerts, C., Bedding, T.R., Christensen-Dalsgaard, J., Eds.; Astronomical Society of the Pacific Conference Series; Astronomical Society of the Pacific: San Francisco, CA, USA, 2002; Volume 259, p. 96.
20. Soydugan, E.; İbanoğlu, C.; Soydugan, F.; Akan, M.C.; Demircan, O. The connection between the pulsational and orbital periods for eclipsing binary systems. *Mon. Not. R. Astron. Soc.* **2006**, *366*, 1289–1294. [CrossRef]
21. Liakos, A.; Niarchos, P.; Soydugan, E.; Zasche, P. Survey for δ Sct components in eclipsing binaries and new correlations between pulsation frequency and fundamental stellar characteristics. *Mon. Not. R. Astron. Soc.* **2012**, *422*, 1250–1262. [CrossRef]
22. Zhang, X.B.; Luo, C.Q.; Fu, J.N. On the Pulsational-Orbital-period Relation of Eclipsing Binaries with δ-Sct Components. *Astrophys. J.* **2013**, *777*, 77. [CrossRef]
23. Liakos, A.; Niarchos, P. Binaries with a δ Scuti Component: Results from a Long-Term Observational Survey, Updated Catalog, and Future Prospects. In *Living Together: Planets, Host Stars and Binaries, Litomyšl, Czech Republic, 8–12 September 2014*; Torres, G., Zejda, M., Eds.; Astronomical Society of the Pacific Conference Series; Astronomical Society of the Pacific: San Francisco, CA, USA, 2015; Volume 496, p. 195.
24. Liakos, A.; Niarchos, P. Poetry in Motion: Asteroseismology of Delta Scuti Stars in Binaries using Kepler Data. In Proceedings of the 12th Hellenic Astronomical Conference, Thessaloniki, Greece, 28 June–2 July 2015.
25. Kahraman Aliçavuş, F.; Soydugan, E.; Smalley, B.; Kubát, J. Eclipsing binary stars with a δ Scuti component. *Mon. Not. R. Astron. Soc.* **2017**, *470*, 915–931. [CrossRef]
26. Liakos, A.; Niarchos, P. Catalogue and properties of δ Scuti stars in binaries. *Mon. Not. R. Astron. Soc.* **2017**, *465*, 1181–1200. [CrossRef]
27. Murphy, S.J. Pulsating stars in binary systems: A review. *arXiv* **2018**, arXiv:1811.12659.
28. Murphy, S.J.; Moe, M.; Kurtz, D.W.; Bedding, T.R.; Shibahashi, H.; Boffin, H.M.J. Finding binaries from phase modulation of pulsating stars with Kepler: V. Orbital parameters, with eccentricity and mass-ratio distributions of 341 new binaries. *Mon. Not. R. Astron. Soc.* **2018**, *474*, 4322–4346. [CrossRef]
29. Shibahashi, H.; Kurtz, D.W. FM stars: A Fourier view of pulsating binary stars, a new technique for measuring radial velocities photometrically. *Mon. Not. R. Astron. Soc.* **2012**, *422*, 738–752. [CrossRef]
30. Shibahashi, H.; Kurtz, D.W.; Murphy, S.J. FM stars II: A Fourier view of pulsating binary stars—Determining binary orbital parameters photometrically for highly eccentric cases. *Mon. Not. R. Astron. Soc.* **2015**, *450*, 3999–4015. [CrossRef]
31. Murphy, S.J.; Shibahashi, H. Deriving the orbital properties of pulsators in binary systems through their light arrival time delays. *Mon. Not. R. Astron. Soc.* **2015**, *450*, 4475–4485. [CrossRef]
32. Liakos, A. Asteroseismology of two Kepler detached eclipsing binaries. *Astron. Astrophys.* **2020**, *642*, A91. [CrossRef]
33. Murphy, S.J.; Pigulski, A.; Kurtz, D.W.; Suárez, J.C.; Handler, G.; Balona, L.A.; Smalley, B.; Uytterhoeven, K.; Szabó, R.; Thygesen, A.O.; et al. Asteroseismology of KIC 11754974: A high-amplitude SX Phe pulsator in a 343-d binary system. *Mon. Not. R. Astron. Soc.* **2013**, *432*, 2284–2297. [CrossRef]
34. Breger, M. δ Scuti stars (Review). In *Delta Scuti and Related Stars, Vienna, Austria, 4–7 August 1999*; Breger, M., Montgomery, M., Eds.; Astronomical Society of the Pacific Conference Series; Astronomical Society of the Pacific: San Francisco, CA, USA, 2000; Volume 210, p. 3.
35. Prša, A.; Batalha, N.; Slawson, R.W.; Doyle, L.R.; Welsh, W.F.; Orosz, J.A.; Seager, S.; Rucker, M.; Mjaseth, K.; Engle, S.G.; et al. Kepler Eclipsing Binary Stars. I. Catalog and Principal Characterization of 1879 Eclipsing Binaries in the First Data Release. *Astron. J.* **2011**, *141*, 83. [CrossRef]
36. Liakos, A.; Niarchos, P. Observations of candidate oscillating eclipsing binaries and two newly discovered pulsating variables. *Commun. Asteroseismol.* **2009**, *160*, 2. [CrossRef]
37. Liakos, A.; Niarchos, P. The oEA stars QY Aql, BW Del, TZ Dra, BO Her and RR Lep: Photometric analysis, frequency search and evolutionary status. *Astrophys. Space Sci.* **2013**, *343*, 123–133. [CrossRef]
38. Liakos, A.; Cagaš, P. First frequency analysis for three new members of the group of eclipsing binaries with a pulsating component. *Astrophys. Space Sci.* **2014**, *353*, 559–566. [CrossRef]
39. Liakos, A. Asteroseismology of Kepler Algol-type oscillating eclipsing binaries. *Astron. Astrophys.* **2017**, *607*, A85. [CrossRef]

40. Liakos, A. KIC 8553788: A pulsating Algol with an extreme mass ratio. *Astron. Astrophys.* **2018**, *616*, A130. [CrossRef]
41. Slawson, R.W.; Prša, A.; Welsh, W.F.; Orosz, J.A.; Rucker, M.; Batalha, N.; Doyle, L.R.; Engle, S.G.; Conroy, K.; Coughlin, J.; et al. Kepler Eclipsing Binary Stars. II. 2165 Eclipsing Binaries in the Second Data Release. *Astron. J.* **2011**, *142*, 160. [CrossRef]
42. Pinsonneault, M.H.; An, D.; Molenda-Żakowicz, J.; Chaplin, W.J.; Metcalfe, T.S.; Bruntt, H. A Revised Effective Temperature Scale for the Kepler Input Catalog. *Astrophys. J. Suppl. Ser.* **2012**, *199*, 30. [CrossRef]
43. Armstrong, D.J.; Gómez Maqueo Chew, Y.; Faedi, F.; Pollacco, D. A catalogue of temperatures for Kepler eclipsing binary stars. *Mon. Not. R. Astron. Soc.* **2014**, *437*, 3473–3481. [CrossRef]
44. Huber, D.; Silva Aguirre, V.; Matthews, J.M.; Pinsonneault, M.H.; Gaidos, E.; García, R.A.; Hekker, S.; Mathur, S.; Mosser, B.; Torres, G.; et al. Revised Stellar Properties of Kepler Targets for the Quarter 1-16 Transit Detection Run. *Astrophys. J. Suppl. Ser.* **2014**, *211*, 2. [CrossRef]
45. Frasca, A.; Molenda-Żakowicz, J.; De Cat, P.; Catanzaro, G.; Fu, J.N.; Ren, A.B.; Luo, A.L.; Shi, J.R.; Wu, Y.; Zhang, H.T. Activity indicators and stellar parameters of the Kepler targets. An application of the ROTFIT pipeline to LAMOST-Kepler stellar spectra. *Astron. Astrophys.* **2016**, *594*, A39. [CrossRef]
46. Qian, S.B.; Li, L.J.; He, J.J.; Zhang, J.; Zhu, L.Y.; Han, Z.T. LAMOST views δ Scuti pulsating stars. *Mon. Not. R. Astron. Soc.* **2018**, *475*, 478–491. [CrossRef]
47. Berger, T.A.; Huber, D.; Gaidos, E.; van Saders, J.L. Revised Radii of Kepler Stars and Planets Using Gaia Data Release 2. *Astrophys. J.* **2018**, *866*, 99. [CrossRef]
48. Bai, Y.; Liu, J.; Bai, Z.; Wang, S.; Fan, D. Machine-learning Regression of Stellar Effective Temperatures in the Second Gaia Data Release. *Astronom. J.* **2019**, *158*, 93. [CrossRef]
49. Davenport, J.R.A. The Kepler Catalog of Stellar Flares. *Astrophys. J.* **2016**, *829*, 23. [CrossRef]
50. Boumis, P.; Meaburn, J.; Goudis, C.D. ARISTARCHOS Instrumentation: Manchester Echelle Spectrometer (MES) and Aristarchos Transient Spectrometer (ATS/PatMan). In Proceedings of the Hellenic Astronomical Society Sixth Astronomical Conference, Athens, Greece, 15–17 September 2003; p. 313.
51. Nelson, B. RaVeRe (Radial Velocity Reductions). 2009. Available online: https://www.variablestarssouth.org/software-by-bob-nelson/ (accessed on 15 August 2020).
52. Joshi, S.; Semenko, E.; Moiseeva, A.; Sharma, K.; Joshi, Y.C.; Sachkov, M.; Singh, H.P.; Yerra, B.K. High-resolution Spectroscopy and Spectropolarimetry of Selected δ-Sct Pulsating Variables. *Mon. Not. R. Astron. Soc.* **2017**, *467*, 633–645. [CrossRef]
53. Cox, A.N. *Allen's Astrophysical Quantities*; Springer: New York, NY, USA, 2000.
54. Prša, A.; Zwitter, T. A Computational Guide to Physics of Eclipsing Binaries. I. Demonstrations and Perspectives. *Astrophys. J.* **2005**, *628*, 426–438. [CrossRef]
55. Wilson, R.E.; Devinney, E.J. Realization of Accurate Close-Binary Light Curves: Application to MR Cygni. *Astrophys. J.* **1971**, *166*, 605. [CrossRef]
56. Wilson, R.E. Eccentric orbit generalization and simultaneous solution of binary star light and velocity curves. *Astrophys. J.* **1979**, *234*, 1054–1066. [CrossRef]
57. Wilson, R.E. Accuracy and efficiency in the binary star reflection effect. *Astrophys. J.* **1990**, *356*, 613–622. [CrossRef]
58. Ruciński, S.M. The Proximity Effects in Close Binary Systems. II. The Bolometric Reflection Effect for Stars with Deep Convective Envelopes. *Acta Astron.* **1969**, *19*, 245.
59. von Zeipel, H. The radiative equilibrium of a rotating system of gaseous masses. *Mon. Not. R. Astron. Soc.* **1924**, *84*, 665–683. [CrossRef]
60. Lucy, L.B. Gravity-Darkening for Stars with Convective Envelopes. *Z. Astrophys.* **1967**, *65*, 89.
61. van Hamme, W. New limb-darkening coefficients for modeling binary star light curves. *Astron. J.* **1993**, *106*, 2096–2117. [CrossRef]
62. Lurie, J.C.; Vyhmeister, K.; Hawley, S.L.; Adilia, J.; Chen, A.; Davenport, J.R.A.; Jurić, M.; Puig-Holzman, M.; Weisenburger, K.L. Tidal Synchronization and Differential Rotation of Kepler Eclipsing Binaries. *Astron. J.* **2017**, *154*, 250. [CrossRef]
63. Liakos, A.; Niarchos, P. A photometric study of the neglected eclipsing binaries: V405 Cep, V948 Her, KR Mon and UZ Sge. *New Astron.* **2012**, *17*, 634–639. [CrossRef]

64. Liakos, A. AbsParEB and InPeVEB: Software for the Calculation of Absolute and Orbital Period Changes Parameters of Eclipsing Binaries. In *Living Together: Planets, Host Stars and Binaries, Litomyšl, Czech Republic, 8–12 September 2014*; Rucinski, S.M., Torres, G., Zejda, M., Eds.; Astronomical Society of the Pacific Conference Series; Astronomical Society of the Pacific: San Francisco, CA, USA, 2015; Volume 496, p. 286.
65. Lenz, P.; Breger, M. Period04 User Guide. *Commun. Asteroseismol.* **2005**, *146*, 53–136. [CrossRef]
66. Schwarzenberg-Czerny, A. An astronomer's guide to period searching. In *Interplay of Periodic, Cyclic and Stochastic Variability in Selected Areas of the H-R Diagram, Brussels, Belgium, 22–24 July 2002*; Sterken, C., Ed.; Astronomical Society of the Pacific Conference Series; Astronomical Society of the Pacific: San Francisco, CA, USA, 2003; Volume 292, p. 383.
67. Montalbán, J.; Dupret, M.A. Effect of convective outer layers modeling on non-adiabatic seismic observables of δ Scuti stars. *Astron. Astrophys.* **2007**, *470*, 991–1002. [CrossRef]
68. Zima, W. FAMIAS—A userfriendly new software tool for the mode identification of photometric and spectroscopic times series. *Commun. Asteroseismol.* **2008**, *157*, 387.
69. Girardi, L.; Bressan, A.; Bertelli, G.; Chiosi, C. Evolutionary tracks and isochrones for low- and intermediate-mass stars: From 0.15 to 7 M_{sun}, and from Z = 0.0004 to 0.03. *Astron. Astrophys. Suppl. Ser.* **2000**, *141*, 371–383. [CrossRef]
70. Soydugan, E.; Soydugan, F.; Demircan, O.; İbanoğlu, C. A catalogue of close binaries located in the δ Scuti region of the Cepheid instability strip. *Mon. Not. R. Astron. Soc.* **2006**, *370*, 2013–2024. [CrossRef]
71. Zacharias, N.; Monet, D.G.; Levine, S.E.; Urban, S.E.; Gaume, R.; Wycoff, G.L. *The Naval Observatory Merged Astrometric Dataset (NOMAD), San Diego, CA, USA, 9–13 January 2005*; American Astronomical Society Meeting Abstracts; American Astronomical Society: Washington, DC, USA, 2004; Volume 205, p. 48.15.
72. Bailer-Jones, C.A.L.; Rybizki, J.; Fouesneau, M.; Mantelet, G.; Andrae, R. Estimating Distance from Parallaxes. IV. Distances to 1.33 Billion Stars in Gaia Data Release 2. *Astronom. J.* **2018**, *156*, 58. [CrossRef]
73. Queiroz, A.B.A.; Anders, F.; Chiappini, C.; Khalatyan, A.; Santiago, B.X.; Steinmetz, M.; Valentini, M.; Miglio, A.; Bossini, D.; Barbuy, B.; et al. From the bulge to the outer disc: StarHorse stellar parameters, distances, and extinctions for stars in APOGEE DR16 and other spectroscopic surveys. *Astron. Astrophys.* **2020**, *638*, A76. [CrossRef]